DESIGN AND IMPLEMENTATION OF ALL-DIGITAL CDMA CODE TRACKING LOOPS

BY

GANIYU BABATUNDE HUSSAIN

A Thesis Presented to the

DEANSHIP OF GRADUATE STUDIES

KING FAHD UNIVERSITY OF PETROLEUM & MINERALS

DHAHRAN, SAUDI ARABIA

In Partial Fulfillment of the
Requirements for the Degree of

MASTER OF SCIENCE

In

Telecommunication Engineering

May 2005

KING FAHD UNIVERSITY OF PETROLEUM & MINERALS
DHAHRAN 31261, SAUDI ARABIA

DEANSHIP OF GRADUATE STUDIES

This thesis, written by **Ganiyu Babatunde Hussain** under the direction of his thesis advisor and approval by his thesis committee, has been presented to and accepted by the Dean of Graduate Studies, in partial fulfillment of the requirements for the degree of **MASTER OF SCIENCE** in **TELECOMMUNICATION ENGINEERING.**

THESIS COMMITTEE

Dr. Al-Andalusi, M.A. (Chairman)

Dr. Zerguine, A. (Member)

Dr. Abuelma'atti, M.T. (Member)

Dr. Jamil M. Bakhashwain
Department Chairman

Dr. Mohammad Abdulaziz Al-Ohali
Dean of Graduate Studies

١٤٢٦/٤/٣٠
Date
7-6-2005

Acknowledgements

In the Name of Allāh, the Most Gracious, the Most Merciful. All praise and thanks is due to Allāh, the Lord of the worlds, who granted me the grace and the health to complete this work. May the peace and blessing of Allāh be upon His Prophet Muhammad *salalau alaihim wasalam.*

Acknowledgement is due to King Fahd University of Petroleum & Minerals for providing the means and opportunity for this study and research.

I express my gratitude and appreciation to my thesis supervisor Dr. Adnan Al-Andalusi for his guidance throughout my thesis. Thanks to my committee members Dr. Azzedine Zerguine and Dr. Muhammad Taher Abuelma'attii for their patience and cooperation in reviewing this thesis.

I give thanks to all the members of the Nigerian community for their support during my stay.

Thanks to my parents, sisters and brother for their love, guidance and support in everything I ever did. May Allāh take excellent care of them and bestow on them mercy.

Contents

List of Tables

List of Figures

ABSTRACT

Name: GANIYU BABATUNDE HUSSAIN

Title: DESIGN AND IMPLEMENTATION OF ALL-DIGITAL CDMA CODE TRACKING LOOPS

Degree: MASTER OF SCIENCE

Major Field: TELECOMMUNICATION ENGINEERING

Date of Degree: MAY 2005

Code Division Multiple Access (CDMA) code tracking performance has been shown to depend on both the correlation properties of the spreading codes and the actual pulse shape utilized. This work quantifies the impact of pulse shaping on the performance of the noncoherent delay lock loop used in code tracking in direct sequence spread spectrum systems. Several families of pulses are considered. The effect of pulse shaping is demonstrated in the presence of multiple access interference. Optimization based on the use of Prolate Spheroidal Wave Functions is carried out to determine optimal pulse shapes in terms of minimum tracking jitter. The optimized pulse shapes are obtained and their performance compared to conventional pulse shapes. Finally, the implementation of the digital tracking loop is carried out using a Digital Signal Processor (DSP).

Keywords: *CDMA, Synchronization, PN code tracking, pulse shape, noncoherent delay lock loop, Prolate Spheroidal Wave Function, DSP.*

King Fahd University of Petroleum & Minerals, Dhahran, Saudi Arabia.

May 2005

خلاصة الرسالة

الأسم : غنيو بابتوندي حسين

عنوان الرسالة: تصميم و نطبيق الكل رقمي لدوائر تتبع رمز ال CDMA.

الدرجة الممنوحة: ماجستير في العلوم

حقل التخصص: هندسة الاتصالات

تاريخ منح الدرجة: مايو 2005م

*لقد تبين ان اداء تتبع رموز*CDMA يتعلق بخصائص التشابه لرموز النشر و شكل النبضة المستعملة. هذا العمل يدرس تاثير شكل النبضة على اداء دائرة الغلق التاخري اللاتزامني المستعملة في تتبع الرموز في انظمة CDMA. لقد تم الاخذ بعين الاعتبارعدة عائلات من الرموز. لقد تم ايضا دراسة تاثير شكل النبضة في وجود التداخل المتعدد الدخول. لقد تم استغلال الامثلة المعتمدة على استعمال دوال الموجة الكروية البرولاتية لتحديد احسن اشكال النبضات و ذلك لامثلة تتبع الاهتزاز الاصغر. لقد تم مقارنة اداء هذه النبضات المطورة بالنبضات التقليدية. اخيرا لقد تم تطبيق هذه الدوائر باستعمال معالج الاشارات الرقمية (DSP).

*مفردات:*CDMA *,تتبع رمز PN. شكل النبضة*, دائرة الغلق التاخري اللاتزامني, دوال الموجة الكروية البرولاتية, معالج الاشارات الرقمية (DSP).

درجة الماجستير في العلوم

جامعة الملك فهد للبترول و المعادن

مايو 2005م

Chapter 1

Background

1.1 Overview of Code Division Multiple Access (CDMA)

Code Division Multiple Access (CDMA) is a multiple access technique used to allow several users to share a communication channel. The sharing of the channel is required to achieve high capacity by simultaneously allocating the available bandwidth to multiple users without severe degradation in the system's performance. Three major multiple access techniques are used to share available bandwidth in a communication system. These are Frequency Division Multiple Access (FDMA), Time Division Multiple Access (TDMA) and Code Division Multiple Access (CDMA) [1].

In FDMA, spectrum is divided up into frequencies and then assigned to users. Only one user at any given time is assigned to a channel. The channel therefore is closed to other conversations until the initial call is finished. TDMA splits frequency into time slots, allowing each user to access the entire communication channel for the short duration the call. Other users share this same frequency channel at different times. If the channel or time slot is not in use in both multiple access technique, it sits idle and cannot be used for other users to increase the system capacity.

CDMA however is based on spread spectrum technology. All users are allowed to occupy all channels at the same time. Transmission is spread over the whole radio band, and each call is assigned a unique code to differentiate it from other calls carried over the same spectrum. Transmission occurs independently and asynchronously with the power transmitted by each user controlled to the minimum required to maintain a given signal-to-noise ratio for the required level of performance. It therefore overcomes the weaknesses of traditional multiple access systems. The unique code utilized in CDMA is called a pseudo-noise (PN) code. PN codes are pseudorandom, meaning that they can be generated mathematically though statistically they nearly satisfy the requirements of a truly random sequence. The PN codes are used to ‘spread’ the narrow band information signal over the whole frequency band and are used by the receiver to ‘despread’ the received signal and recover the original narrow band information signal. This makes the transmitted signals of the other users appear as additive noise. Though there is additional interference when compared to traditional multiple access techniques, the resulting capacity is significantly increased [2].

The following features unique to CDMA are discussed next: universal frequency reuse, use of rake receivers, power control, soft hand off and soft capacity.

A frequency channel can be used again within an FDMA or TDMA network, but cells using the same frequency must be separated by an appropriate distance. Adjacent cells must be assigned a different set of frequencies. As a result, each cell in the site is able to use only a fraction of the possible frequencies. Cells in a CDMA network use all available frequencies and adjacent cells can transmit at the same frequency because users are separated by code channels, not frequency channels. This universal frequency reuse feature of CDMA, termed “frequency reuse of one”, eliminates the need for frequency planning.

Signals sent over the air can take several other paths to the receiver apart from the direct path. These different paths, called multi-paths, can result in the receiver getting several versions of the same signal but at slightly different delays. Multi-paths can cause a loss of signal through cancellation in other multiple access techniques. CDMA however is robust to multi-path. This property is due to the fact that the delayed versions of the transmitted PN signal will have a poor correlation with the original PN code and will appear as another uncorrelated user [1]. In addition, CDMA uses a rake receiver to mitigate the effect of multi-path by identifying the strongest multi-path signals and combining them to produce an even stronger signal. It therefore turns the multi-path problem in other multiple access techniques into an advantage.

Power control is a CDMA feature that enables receivers to adjust the power at which they transmit. If all mobiles transmit at the same power level, the base station will receive unnecessarily strong signals from mobiles nearby and extremely weak signals from mobiles that are far away. This problem is called the near-far problem. Power control ensures that the base station receives all signals at the appropriate power level.

Handoff is the process of transferring a call from one cell to another as the receiver moves between cells. CDMA uses soft handoff. A soft handoff establishes a connection with the new cell prior to breaking the connection with the old cell. This is possible because adjacent CDMA cells use the same frequency. The receiver detects a new pilot as it travels to the next coverage area and establishes the connection with the new cell while the receiver maintains the link with the old cell. Soft handoff is therefore termed a "make-before-break" handoff. Other multiple access techniques use hard handoff where the connection is terminated at the old cell before a new connection is made with the new cell. Hard handoff can increase the likelihood of a dropped call. CDMA is also said to have a 'soft' capacity limit. Increasing the number of users in a CDMA system raises the noise floor in a linear manner [1]. Thus there is no absolute limit on the number of users in a CDMA system. Rather the system performance gradually degrades for all users as the number of users increase.

Other merits of CDMA include privacy, low probability of interception (security) and resistance to narrowband jamming [3]. CDMA has therefore become most popular

signaling scheme and is widely adopted for the third generation (3G) wireless cellular networks [4].

1.2 Synchronization in CDMA

Spread spectrum systems employ the same basic elements of a conventional digital communication system. Conventional digital communication systems require carrier synchronization to take care of frequency and phase differences between the received signal and the signal that is expected at the receiver. In addition to this, spread spectrum systems require ‘code’ synchronization. Code synchronization is used to synchronize in time the code received from the transmitter with the code generated at the receiver. Figure (1-1) shows a generic spread spectrum system with the PN sequence generator at the transmitter and the receiver.

Synchronization of the PN sequences generated at the receiver with the PN sequences contained in the received signal is required in order to properly despread the received spread spectrum signal. At the receiver therefore, carrier phase, frequency and code timing have to be properly synchronized to the received signal for accurate detection of the transmitted information. In a practical system, synchronization is established prior to the transmission of the information by transmitting a fixed PN bit pattern which is designed so that the receiver will detect it with high probability in the presence of interference [5]. After time synchronization of the PN sequence is established, the transmission of information starts.

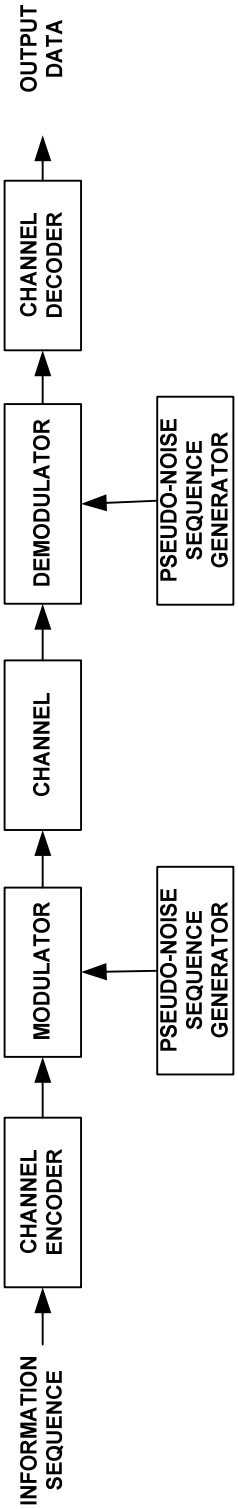

Figure 1-1 : Spread Spectrum System

Efficiency of the spread spectrum system is highly dependent on the capability of the receiver to continuously maintain this synchronization between the received signal PN code and the locally generated PN codes. Several analyses have been made on the performance of CDMA systems with the assumption that there is perfect PN synchronization. However PN synchronization is one of the most difficult tasks in spread spectrum communication systems. Synchronization of the receiver to the received spread spectrum signal is separated into two distinct phases: code acquisition and code tracking.

1.2.1 Code Acquisition

During acquisition, the receiver obtains the relative delay between the received signal and the locally generated code to within a code chip interval. The normalized delay error between the input and local sequence is made less than one.

The usual procedure for establishing initial synchronization is for the transmitter to send known pseudo-noise data sequence to the receiver [5]. The receiver is continuously in search for this known sequence in order to establish initial synchronization. There is no prior knowledge of the received signal hence the sequence must be searched by testing different phases of the internal sequence against the received signal. The matched filter or cross correlation are the optimum methods for estimating delay and for establishing initial synchronization. A filter matched to the known data waveform generated from the known pseudorandom sequence continuously looks to exceed a predetermined threshold.

When this threshold is exceeded, initial synchronization is established and the demodulator starts the tracking mode.

Alternatively, a sliding correlator may be used. The correlator cycles through time uncertainty, usually in discrete time intervals of half a chip interval and correlates the received signal with the known synchronization sequence. Cross correlation is performed over the whole time interval. The correlator output is compared with a threshold to determine if the known signal sequence is present. If the threshold is not exceeded, the known reference signal is advanced in time by half a chip interval and the correlation process is repeated. These operations are performed until a signal is detected or until the search has been performed over the whole time uncertainty interval [6].

There are different approaches to these operations with different acquisition times and complexities. The least complex, but the slowest is the completely serial algorithm which tests each phase of the internal sequence against the received signal. The most costly and complex, though also fastest, is the completely parallel algorithm where different phases of the sequence are compared simultaneously. In practice however total parallelism is out of the question when the sequence is very long and simpler solutions are necessary. Between these two extreme solutions there are a variety of hybrids using different degrees of parallelism.

1.2.2 Code Tracking

Further adjustment to remove the slight misadjustment left and fine tune the delay to as close to zero as possible is done during tracking. The development of closed loop techniques for accurate PN tracking plays an important role in supporting the acquisition process once the code has been acquired. The optimum design and true assessment of the performance of the PN tracking loop is an essential component of the overall receiver design [7]. If the received signal is out of synchronism by a fraction of a chip, insufficient signal energy will reach the demodulator resulting in inaccurate detection of the transmitted information. The tracking process is the focus of this work.

Code tracking is accomplished using phase-locked techniques similar to those utilized for carrier tracking. The principal difference between the phase-locked loop techniques used for carrier tracking and those used in code tracking is the implementation of the phase discriminator [8]. Unlike the implementation of the phase discriminator in code tracking, traditional phase-locked loop techniques employ several multipliers, pairs of filters and envelop detectors. The phase discriminator utilized in code tracking makes use of correlation operations between the received signal and the two different phases, early and late, of the receiver generated spreading waveform.

A tracking loop that makes use of the independent correlators is called a delay-lock tracking loop (DLL) [9-12]. The loop that time shares a single correlator is called a Tau-dither tracking loop (TDL) [12, 13]. Either of these configurations can be operated in a

coherent or noncoherent mode depending on the system application [7]. Coherent loops make use of the receiver carrier phase information while noncoherent loops do not. Both the full-time delay lock loop and time-shared delay lock loop tracking loops use the early-late gate structure [10]. They maintain synchronization of the receiver's replica of the spreading code by using two correlators called an early correlator and a late correlator.

An early correlator uses a code reference waveform that is advanced in time by some fraction of a chip with respect to the currently estimated code phase. A late correlator uses a code reference waveform that is delayed by some fraction of a chip. The difference between the early and late correlations is used to sense small deviations of the incoming spreading code's timing with respect to the early and late code timing. If the synchronism is not exact, the filtered output from one correlator will exceed the other and a voltage controlled oscillator (VCO) will be appropriately advanced or delayed. The VCO is a clock in the sense that it drives the PN code generator such that when the PN code generator clock is lagging in phase in comparison with the incoming sequence phase, it drives the clock faster and vice versa. At equilibrium point, the two filtered correlator outputs will be equally displaced from the peak value and the PN code generator output will be exactly synchronized to the received signal that is fed to the demodulator [6]. Once the sequence timing is acquired and tracked accurately, the spreading can be removed.

1.3 Thesis Motivation

Code Division Multiple Access (CDMA) has become important in the field of communication and several benefits are obtained from using it when compared to traditional multiple access schemes. The important aspect of a CDMA system is the pseudo-noise codes (PN codes) used. Two aspects of these codes have an effect on the performance of the communication system as a whole, their correlation property and their chip pulse shape. Several studies have been done to investigate the effect of the correlation property of the PN codes and many code sequences have been proposed which improve the performance of synchronization in a CDMA system. The chip pulse shape on the other hand is also known to have an effect on the performance of synchronization in CDMA system. Proper pulse shaping improves the spectral performance of the modulation scheme used. This improves the bandwidth efficiency allowing longer spreading codes to be used in the system to accommodate a larger number of users at a given error level or the same number of users at less error level. This motivated the study of the effect of different chip pulse shaping techniques in code tracking of CDMA synchronization.

1.4 Thesis Contribution

The objective of this thesis is to investigate the effect of different pulse shapes on code tracking. The effect of the correlation properties of the spreading codes is neglected by assuming random codes thereby focusing on the actual PN pulse shape. Earlier works that have improved on the performance of the code tracking loop have focused on modifying the structure of the loop itself. We have kept the structure of the loop intact but instead improved on the performance of the loop by varying the PN code pulse shape. Some work has been done on choosing other pulse shapes apart from the standard rectangular pulse shape and studying the effect they have on the coherent delay lock loop. This work however quantifies the effect of different pulse shapes on the more practical noncoherent delay lock loop.

In addition, an optimization work is formulated to find pulse shapes with optimum tracking capabilities in terms of minimum tracking error. Earlier work on pulse shape optimization applied to CDMA code tracking loops have only been done for the coherent delay lock loop. This work extends pulse shape optimization for the noncoherent delay lock loop. Optimized pulse shapes provide a new design for the noncoherent delay lock loop. It should be noted that this new design can be applied to any previous work on modified loop structure to provide even better performance. Finally, a digital signal processor (DSP) implementation is done to validate some theoretical results and to demonstrate practical ways of implementing the new design in hardware.

1.5 Previous Work

In several papers the delay lock loop (DLL) has been analyzed. The earliest work on code tracking discriminators was done by Spilker and Magill [9] where it was shown that the proper error signal for tracking could be derived from a correlation of the received signal with a receiver generated first derivative of the spreading waveform. Later work by Spilker [10] discussed the theory of operation and evaluation of the performance of a DLL in the presence of additive white Gaussian noise. The work by Gill [11] extended this work and derived the tracking performance for the coherent and noncoherent implementations. A consistent 3dB advantage was obtained using bi-phase modulation (BPSK $d(t) = \{+1,-1\}$) rather than on-off keying (ASK $d(t) = \{0, \sqrt{2}\}$) at the expense of more complexity.

Hartmann [13] analyzed the performance for a tau-dither loop (TDL) in the presence of white Gaussian noise and based his analysis on variance and code delay error. A square-law envelope detector (noncoherent) is used. The signal to noise performance of the TDL loop is approximately 3dB worse because of the time-sharing of the early and late correlators. The results were derived under the assumption of additive white Gaussian noise at the input of the loop.

Meyr [14-16] was first to introduce the idea of modeling the stochastic time evolution of the phase error in a tracking loop as a renewal Markov process. Unlike the carrier tracking loop where the nonlinear phase error characteristic is periodic, code tracking

loop have an essentially aperiodic phase error characteristic, of finite range and with the error process driven by additive noise bound to reach a finite boundary within a finite time when the loop loses lock. They can therefore be modeled using the renewal theory approach. Polydoros and Weber [17] applied this renewal theory to the study of the aperiodic finite phase error characteristic for the case of a noncoherent delay lock loop. The exact renewal theory approach is compared to the approximate periodic extension approach and it is found that for low signal-to-noise ratio (SNR), the exact and approximate theories could deviate while at high SNR they yield identical performance.

Simon [12] performed the optimum design and performance of the noncoherent DLL and TDL configurations, investigating the band limiting effect of the bandpass arm filters and demonstrating that for some fixed data rate and SNR, there exists an optimum filter bandwidth in the sense of minimizing the loops tracking jitter.

Coherent loops are discussed in [10, 11] while the more practical Noncoherent loops are discussed in [11-13, 18]. Noncoherent loops are important because they are relatively insensitive to data modulation and do not presume reliable carrier tracking prior to PN code acquisition as do coherent loops [19]. The performance analysis of the conventional noncoherent DLL (NCDLL) for additive white Gaussian noise channels was done in [17], using the linear and nonlinear approaches. The linear approach is used at high SNR while the nonlinear approach is used at low SNR. The nonlinear approach uses the renewal theory process by [15].

Work has been done to enhance the performance of the DLL by modifying the DLL structure. A modified noncoherent DLL was first introduced by Yost and Boyd [18] . The loop was shown to have a superior tracking performance to the traditional DLL. They further considered the band-limiting effects of the bandpass arm filters on the performance of the modified DLL demonstrating its increased performance below a certain SNR. The extended tracking range DLL proposed by [20] increases the loop noise thereby increasing the jitter performance and reducing the noise power. Further improvement on the work by Yost and Boyd was done by [21] where the proposed design increases the number of correlations by addition of two new phase shifted PN reference signals, advanced and delayed by a period, thus allowing the loop discriminator characteristics to be shaped in such a way as to expand the loops correlation range without affecting the lock-in range.

The performance of the conventional NCDLL is degraded in the presence of Doppler shift as highlighted by [19, 22] and in the presence of multi-path fading as highlighted by [23, 24]. Some new code tracking loops have been proposed and developed to combat multipath fading including the multipath estimating delay lock loop [25] and the rake delay lock loop [26].

Most of these earlier modifications focus on the structure of the DLL [18, 20, 21, 27] which change the phase error characteristic (S-curve). Chip pulse shaping for specific early-late spacing on the other hand has an effect on the S-curve.

The effect of non rectangular despreading was undertaken by [28]. The performance of a coherent delay-locked tracking scheme for CDMA using half-sine and triangular chip waveforms for early and late despreading was analyzed. Conventional chip waveform shapes use rectangular pulses. The root mean square (RMS) tracking error of this coherent DLL is compared to the conventional DLL. The root mean square tracking error is obtained by linear loop analysis given in [8]. The results show that the use of both the half-sine and the triangular chip waveform for despreading reduces the RMS tracking error. The effect of unmatched despreading was undertaken by [29]. Unmatched despreading chip waveform for locally generated early and late despreading codes in a coherent delay lock loop (CDLL) was considered. The performance of the DLL was evaluated using linear and nonlinear theories and an optimum despreading chip waveform was pursued in the sense of minimizing the root mean square (RMS) tracking error. Both the rectangular and sinc waveforms were used and it was found that despreading chip waveforms are optimum for any specified early-late discriminator offset. Comparison was made between the conventional CDLL and the proposed CDLL with optimized despreading chip waveform.

Optimization of pulse shapes for CDMA to minimize the multiple access interference power under various constraints including bandwidth occupancy, continuous signal phase and constant envelope was undertaken in [30, 31]. The method using Prolate Spheroidal Wave Functions was applied to the CDLL in [32]. This work extends the effects of pulse shaping to the Noncoherent DLL and applies the optimization method developed in [30, 32] to pulse shapes for the Noncoherent DLL.

1.6 Thesis Organization

This thesis is organized in the following manner:

(i). Chapter 2 discusses the system models for CDMA, digital phase lock loops and code tracking loops. The system models are used later as a basis for the analysis of the performance of code tracking loops.

(ii). Chapter 3 discusses pulse shaping. First the root mean square tracking error and mean-time-to-lose lock are introduced as performance measures used for code tracking. Next the tracking performance for various pulse shapes is quantified and the numerical results obtained are presented.

(iii). Chapter 4 formulates the optimization problem. The method used in solving it is discussed and solutions reached are presented.

(iv). Chapter 5 discusses the implementation in hardware using digital signal processors.

(v). Chapter 6 concludes with a summary and suggestion for future work.

(vi). Appendix A gives detail description of the formulation of the mean and variance tracking statistics and Appendix B describes the digital signal processor used.

Chapter 2

System Models

This chapter discusses the system models for CDMA, digital phase lock loop and code tracking loops. The model for CDMA describes the signals, how they are modulated and transmitted, and components of the received signal including the PN code sequence. Linear model of the digital phase lock loop (DPLL) is analyzed to get the expression for the closed loop transfer function. The DPLL analysis forms the basis for the analysis of the code tracking loops. The code tracking loop model is then presented for the coherent delay lock loop and the noncoherent delay lock loop with the loop error characteristic derived for both. The linear loop analysis for the DPLL and the loop error characteristic of the Noncoherent delay lock loop are used for performance analysis of the tracking loop and to demonstrate the effect of pulse shaping.

2.1 CDMA System Model

In CDMA, the PN sequence generated at the modulator is used in conjunction with the phase shift keying (PSK) modulation to shift the phase of the PSK signal pseudo randomly at the rate that is an integer multiple of the bit rate. PSK is appropriate in applications where phase coherence between the transmitted signal and the received signal can be maintained over a time interval that is relatively long compared to the reciprocal of the transmitted signal bandwidth [6].

For simplicity, consider the transmission of a binary information sequence by means of binary PSK (BPSK) with information rate R bits/sec and the bit interval $T_b = 1/R$ seconds. Figure (2-1) shows a BPSK spread spectrum modulator and demodulator. The available channel bandwidth is B_c Hz, where $B_c >> R$. At the modulator, the bandwidth of the information signal is expanded to $W = B_c$ Hz by shifting the phase of the carrier pseudo randomly at a rate of W times/sec according to the PN sequence. The received baseband CDMA is expressed as:

$$r(t) = \sqrt{2P}c(t-\tau_o)d(t-\tau_o) + n(t) \qquad (2\text{-}1)$$

where P is the signal power, τ_o is the propagation delay, $d(t)$ is the binary data sequence of independent identically distributed symbols selected from the alphabet $\{-1,+1\}$ and $n(t)$ is additive white noise process with two-sided power spectral density

equal to $N_o/2$ w/Hz. The information bearing binary data sequence denoted by $d(t)$ is multiplied by the signal from the PN sequence generator, which is expressed as:

$$c(t) = \sum_{n=-\infty}^{\infty} c_n h(t - nT_c) \qquad (2\text{-}2)$$

where $\{c_n\}$ represents the binary PN code sequence of constant zero mean independent binary random variables ± 1. $h(t)$ is any chip pulse shape of duration T_c. The product signal $d(t)c(t)$ is used to amplitude modulate the carrier $\sqrt{2P}\cos\omega_c t$. By multiplying the received signal with a synchronized replica of the PN code signal, the desired signal is despread back to a narrow bandwidth while any interference signal is spread over the wide bandwidth. The net effect is a reduction in the interference power by the factor W/R, which is called the processing gain of the spread-spectrum system. The PN code sequence $\{c_n\}$ is assumed to be known only to the intended receiver. Any other receiver that does not have knowledge of the PN code sequence cannot demodulate the signal. Consequently, the use of a PN code sequence provides a degree of security that is not possible to achieve with traditional multiple access techniques. The cost of this security and performance gain against interference is increased channel bandwidth utilization.

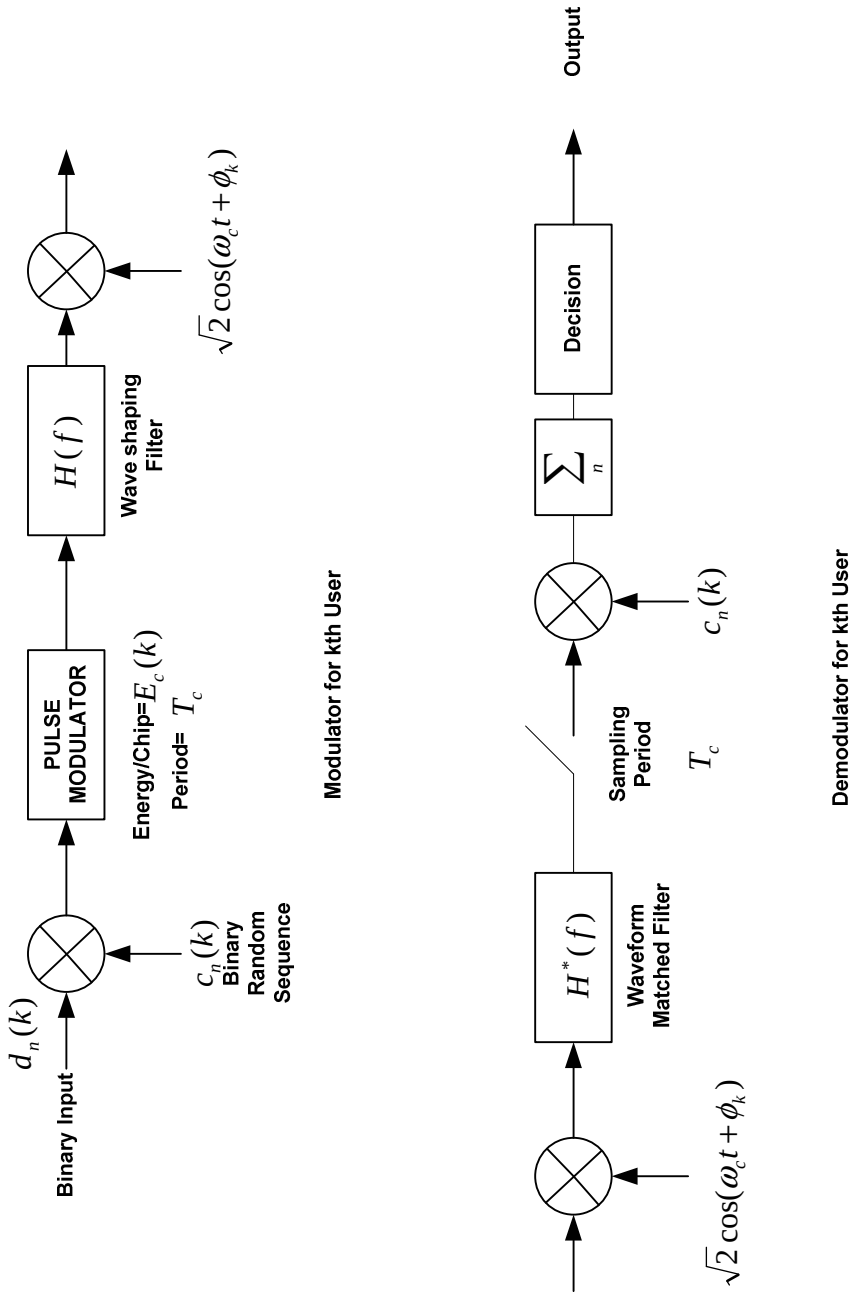

Figure 2-1 : BPSK Spread Spectrum Modulator-Demodulator

2.2 Digital Phase Locked Loop

The earliest work on code tracking discriminator [9] follows the scheme of a phase-locked loop that tracks the phase of a carrier. The phase-locked loop is shown in Figure (2-2). The authors showed that the proper signal for tracking could be derived from a correlation of the received signal with a receiver generated first derivative of the spreading waveform. The conventional phase-locked loop (PLL) employs this same method. The PLL is the basic element of any configuration of code tracking system. The linear model of the digital phase-locked loop is therefore used in modeling digital code tracking loops.

In a conventional PLL, the input signal $\sin(\omega_o t + \theta)$ is correlated with a signal $\cos(\omega_o t + \bar{\theta})$, which is the derivative of the received signal. By comparison with Figure (2-2), the digital phase locked loop (DPLL) can be represented as in Figure (2-3).

Assuming we have an input signal $y(t)$ consisting of the received signal and additive noise sampled at regular time instances t_k, we have:

$$y_k = r_k + n_k \qquad (2\text{-}3)$$

$$r_k = A\sin(\omega_o t_k + \theta) \qquad (2\text{-}4)$$

If the control is performed in accordance with:

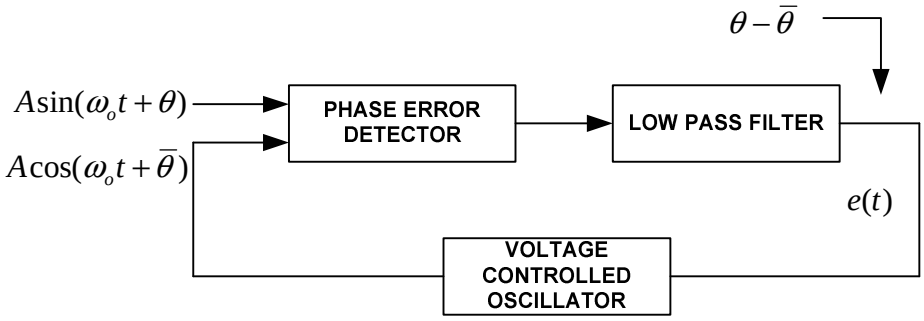

Figure 2-2 : Phase Lock Loop Model

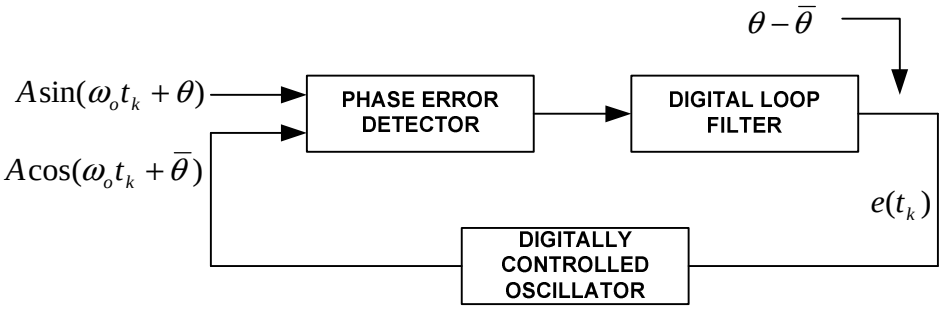

Figure 2-3 : Digital PLL Model

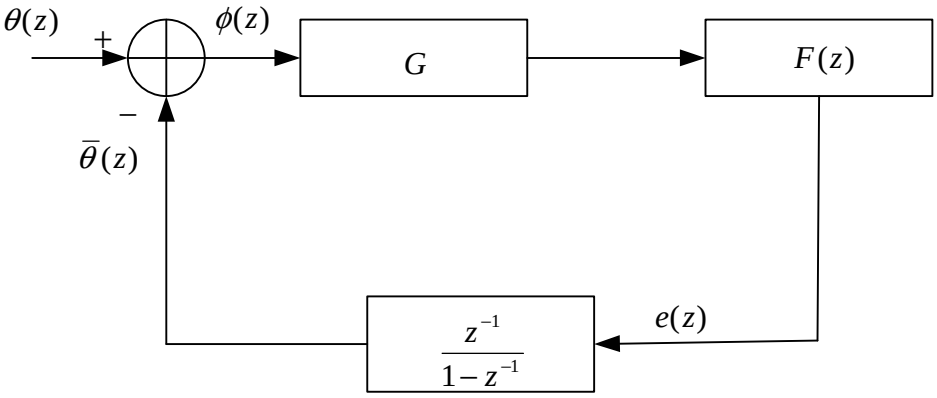

Figure 2-4 : Linear model for Digital PLL

$$\bar{\theta}_{k+1} = \bar{\theta}_k + e(t_k) \tag{2-5}$$

using a z-transform with z^{-1} representing unit delay equal to the sampling interval, we have $z^{-1}\theta_k = \theta_{k-1}$. The previous Equation (2-5) becomes [5]:

$$\bar{\theta}(z) = z^{-1}\bar{\theta}(z) + z^{-1}e(z) \tag{2-6}$$

$$\bar{\theta}(z) = \frac{z^{-1}}{1 - z^{-1}} e(z) \tag{2-7}$$

The equivalent model for the DPLL is shown in Figure (2-4). G is the phase detector nonlinearity function, $F(z)$ is the digital filter transfer function and $z^{-1}/(1 - z^{-1})$ is the digitally controlled oscillator transfer function. From this model $\bar{\theta}(z)$ is expressed as:

$$\bar{\theta}(z) = \frac{GF(z)z^{-1}}{1 - z^{-1}} \phi(z) \tag{2-8}$$

$$\bar{\theta}(z) = \frac{GF(z)}{z - 1} \phi(z) \tag{2-9}$$

The tracking error $\phi(z)$ can be evaluated as:

$$\phi(z) = \theta(z) - \bar{\theta}(z) \tag{2-10}$$

$$\phi(z) = \theta(z) - \frac{GF(z)}{z - 1} \phi(z) \tag{2-11}$$

$$\phi(z)\left[1 + \frac{GF(z)}{z - 1}\right] = \theta(z) \tag{2-12}$$

$$\phi(z) = \left[\frac{(z - 1)}{(z - 1) + GF(z)}\right] \theta(z) \tag{2-13}$$

The above Equation (2-13) is rewritten as:

$$\phi(z) = \left[1 - \frac{GF(z)}{(z-1) + GF(z)}\right]\theta(z) \qquad (2\text{-}14)$$

$$\phi(z) = [1 - H(z)]\theta(z) \qquad (2\text{-}15)$$

By comparison with Equation (2-8)

$$\phi(z) = \left[1 - \frac{\bar{\theta}(z)}{\theta(z)}\right]\theta(z) \qquad (2\text{-}16)$$

$$\frac{\bar{\theta}(z)}{\theta(z)} = H(z) = \frac{GF(z)}{(z-1) + GF(z)} \qquad (2\text{-}17)$$

$H(z)$ is the closed loop transfer function. This linear model will be used in modeling the code tracking loops when evaluating their performance.

2.3 Delay Lock Tracking Loops

A block diagram of a baseband delay lock tracking loop is shown in Figure (2-5). The received signal consisting of a spreading waveform with average signal power *P* and additive white Gaussian noise $n(t)$ with two-sided power spectral density $N_o / 2$ W/Hz is:

$$r(t) = \sqrt{P}c(t - \tau_o) + n(t) \qquad (2\text{-}18)$$

Considering the output of the delay lock discriminator as a static phase measuring device in a noiseless environment, the early-correlator output is:

$$z_1(\tau) = K\sqrt{\frac{P}{2}}c(t - \tau_o)c\left(t - \bar{\tau}_o + \Delta\right) \qquad (2\text{-}19)$$

while the late-correlator output is:

$$z_2(\tau) = K\sqrt{\frac{P}{2}}c(t - \tau_o)c\left(t - \bar{\tau}_o - \Delta\right) \qquad (2\text{-}20)$$

where the delay error $\tau = (\tau_o - \bar{\tau}_o)$, τ_o is the propagation delay, $\bar{\tau}_o$ is the receiver estimate of the propagation delay and Δ represents the time difference between the early and the late discriminator channels $0 < \Delta \le T_c$. The delay lock error signal is the difference between $z_2(\tau)$ *and* $z_1(\tau)$:

$$z_\Delta(\tau) = z_2(\tau) - z_1(\tau) \qquad (2\text{-}21)$$

$$z_\Delta(\tau) = Kc(t - \tau_o)\left[c(t - \bar{\tau}_o - \Delta) - c(t - \bar{\tau}_o + \Delta)\right] \qquad (2\text{-}22)$$

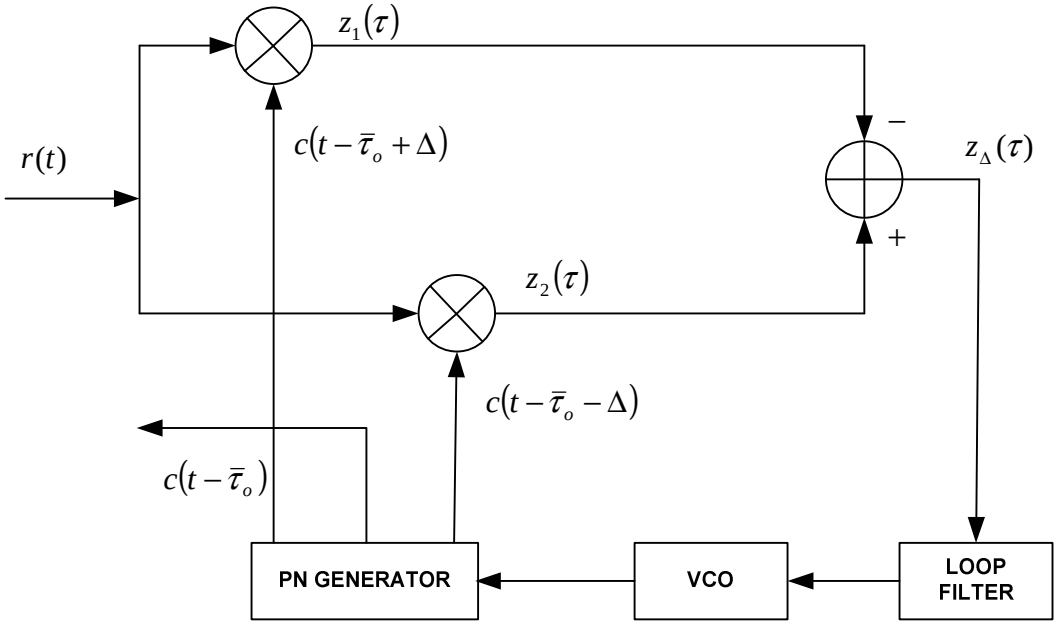

Figure 2-5 : Baseband Delay Lock Tracking Loop

Averaging over NT_c the whole period of $c(t)$ where N is the number of accumulated chips:

$$z_{\Delta}(\tau) = \frac{1}{NT_c} \int_0^{NT_c} Kc(t-\tau_o)\left[c(t-\bar{\tau}_o-\Delta)-c(t-\bar{\tau}_o+\Delta)\right]dt \qquad (2\text{-}23)$$

applying the definition of autocorrelation function:

$$R(\tau) = \frac{1}{NT_c} \int_0^{NT_c} c(t)c(t+\tau)dt \qquad (2\text{-}24)$$

From which the error signal becomes:

$$z_{\Delta}(\tau) = K\left[\frac{1}{NT_c} \int_0^{NT_c} c(t-\tau_o)c(t-\tau_o-\Delta)dt - \frac{1}{NT_c} \int_0^{NT_c} c(t-\tau_o)c(t-\tau_o+\Delta)dt\right] \qquad (2\text{-}25)$$

$$z_{\Delta}(\tau) = K\left[R(\tau_o-\bar{\tau}_o-\Delta)-R(\tau_o-\bar{\tau}_o+\Delta)\right] \qquad (2\text{-}26)$$

substituting for the delay error $\tau = (\tau_o - \bar{\tau}_o)$:

$$z_{\Delta}(\tau) = K\left[R(\tau-\Delta)-R(\tau+\Delta)\right] \qquad (2\text{-}27)$$

The discriminator S-curve of the baseband DLL is obtained to be proportional to:

$$G(\tau) = R(\tau-\Delta)-R(\tau+\Delta) \qquad (2\text{-}28)$$

We define the normalized chip timing error ε as:

$$\varepsilon = \frac{\tau}{T_c} \qquad (2\text{-}29)$$

and the normalized time difference between the early and late discriminator channels, the early-late discriminator offset δ as:

$$\delta = \frac{\Delta}{T_c} \tag{2-30}$$

The early and late PN signals are $2\delta T_c$ apart and a loop such as this is said to have δ of correlator spacing. Equation (2-28) above becomes:

$$G\left(\frac{\tau}{T_c}\right) = R\left(\frac{\tau - \Delta}{T_c}\right) - R\left(\frac{\tau + \Delta}{T_c}\right) \tag{2-31}$$

$$G(\varepsilon) = R(\varepsilon - \delta) - R(\varepsilon + \delta) \tag{2-32}$$

The coherent DLL in Figure (2-6) is based on the same early-late gate structure but with the effect of data removed through multiplication with the estimated bits after the delay block. Similarly the discriminator S-curve of the coherent DLL is obtained as [8]:

$$G(\varepsilon) = R(\varepsilon - \delta) - R(\varepsilon + \delta) \tag{2-33}$$

The discriminator S-curve for the coherent DLL is shown in Figure (2-7) for the case of a Rectangular pulse shape at early-late discriminator offset δ = 0.5 and 1.

In most practical applications, the input signal to the tracking loop will be a complete spread spectrum signal including the actual data. The tracking loop input must be recovered from the carrier, that is the received signal must first be demodulated. Spread spectrum systems typically operate at low signal-to-noise ratios in the transmission bandwidth making demodulation difficult as a coherent carrier reference must be generated prior to demodulation. In order to remove this difficulty in practical systems, a noncoherent delay lock tracking is used with two energy detectors which are not sensitive

to data modulation or carrier phase and thus enable the demodulator to ignore data modulation and carrier phase. The noncoherent delay lock loop (NCDLL) is shown in Figure (2-8).

The received signal $r(t)$ is cross-correlated with the early and late versions of the local PN codes generator sequence. The results of these cross-correlation operations are then band-pass filtered, square-law envelope detected and differenced to produce an error (discriminator) characteristic. The loop is closed by applying this differentiated output to a loop filter and voltage controlled oscillator (VCO) that drives the PN code generator from which the PN reference sequence is obtained. The output of the squaring circuit has one component at baseband and another double frequency component which is rejected by the cascade of the filter and voltage controlled oscillator (VCO). The received signal consisting of a spreading waveform with average signal power P is expressed as:

$$r(t) = \sqrt{2P}c(t-\tau_o)d(t-\tau_o)\cos\left(\omega_o t + \phi(t)\right) + n(t) \qquad (2\text{-}34)$$

where

P = received signal power

τ_o = propagation delay

$\phi(t)$ is the random phase of the carrier

and $n(t)$ is white Gaussian noise represented as:

$$n(t) = n_c(t)\sqrt{2}\cos\left(\omega_o t + \phi(t)\right) - n_s(t)\sqrt{2}\sin\left(\omega_o t + \phi(t)\right) \qquad (2\text{-}35)$$

where $n_c(t)$ and $n_s(t)$ are lowpass white noise waveforms that are statistically independent stationary Gaussian processes with two-sided power spectral density equal

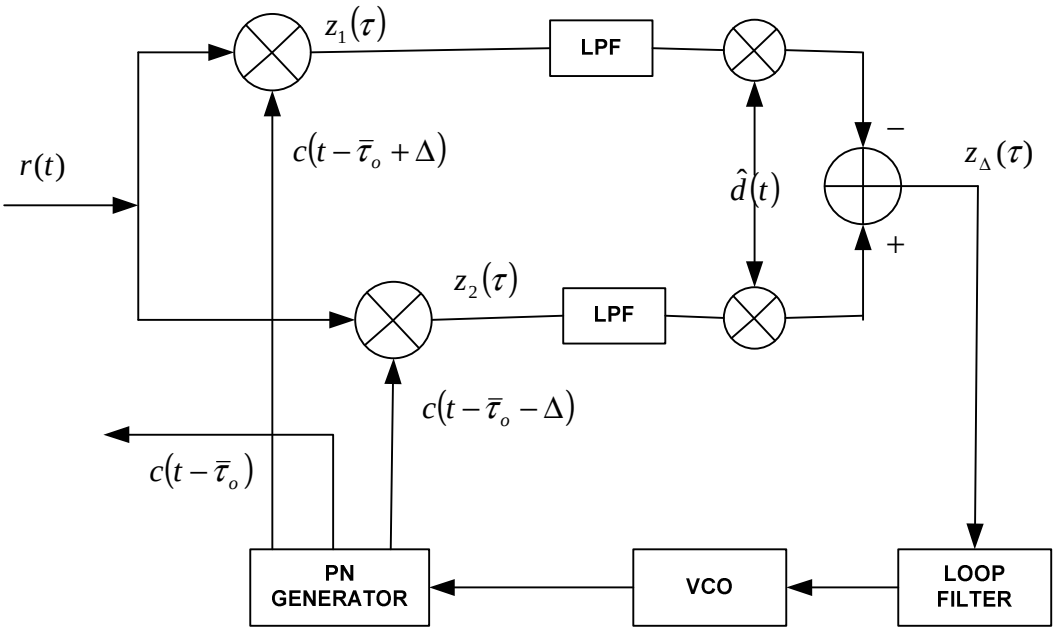

Figure 2-6 : Coherent delay lock tracking Loop

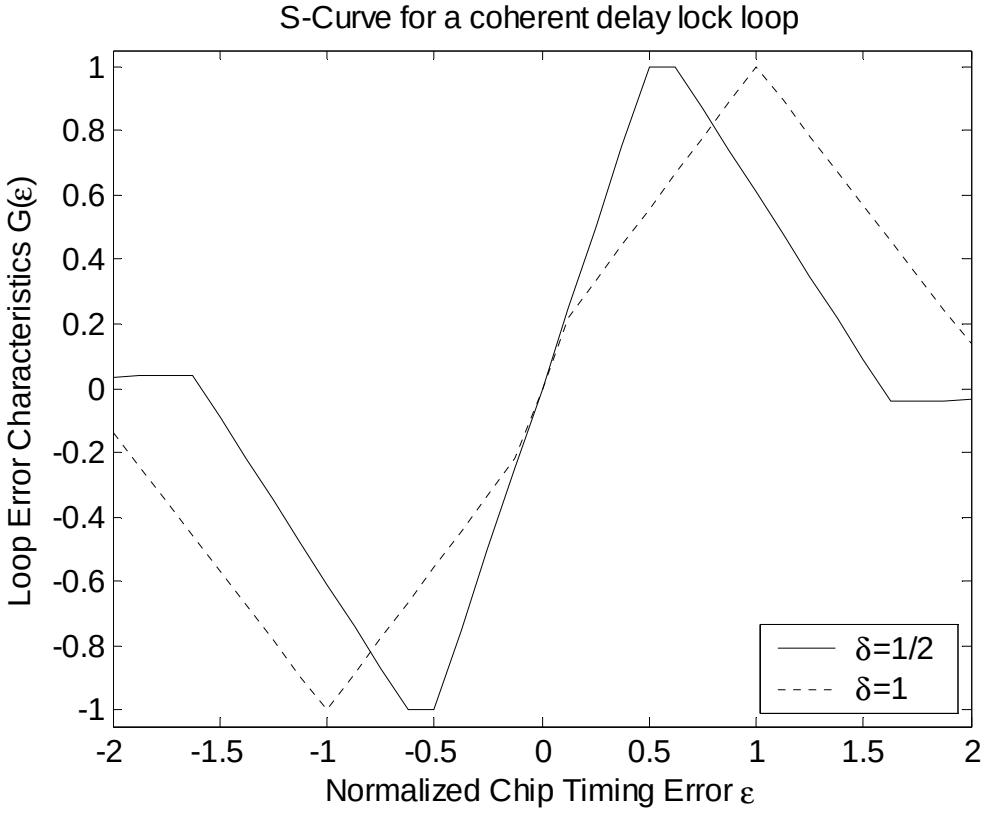

Figure 2-7 : Coherent DLL S-curve using Rectangular Pulse Shape

to $\frac{N_o}{2}$ w/Hz. The error signal $z_\Delta(\tau)$ is the difference of the squared envelope of the two signals, each multiplied by early and late PN codes respectively.

Considering the case for QPSK, the received signal has the form:

$$r(t) = \sqrt{2P}d(t-\tau_o)\left\{c_I(t-\tau_o)\cos\left(\omega_o t+\phi(t)\right)+c_Q(t-\tau_o)\sin\left(\omega_o t+\phi(t)\right)\right\}+n(t) \quad (2\text{-}36)$$

where $c_I(t)$ and $c_Q(t)$ are two independent I (in phase) and Q (quadrature phase) channel PN sequences. The output of the band pass filter (BPF) on the I channel is:

$$x_i(t) = \left[r(t)c_I(t-\tau_o \pm \Delta)\right]_{BPF} \quad (2\text{-}37)$$

$$x_i(t) = \sqrt{2P}K_i\,\overline{d(t-\tau_o)}\;\overline{c_I(t-\tau_o)c_I(t-\bar{\tau}_o \pm \Delta)}\cos\left(\omega_o t+\phi(t)\right)+N_i(t) \quad i=1,2 \quad (2\text{-}38)$$

where

$$N_i(t) \underline{\underline{\Delta}} \sqrt{2P}K_i\,\overline{d(t-\tau_o)}\;\overline{c_Q(t-\tau_o)c_I(t-\bar{\tau}_o \pm \Delta)}\sin\left(\omega_o t+\phi(t)\right)+\overline{n(t)c_I(t-\bar{\tau}_o \pm \Delta)} \quad i=1,2$$

$$\overline{d(t-\tau_o)} = \frac{1}{T_c}\int_0^{T_c} d(t-\tau_o)dt = 1 \quad (2\text{-}39)$$

$$\begin{aligned}\overline{c_I(t-\tau_o)c_I(t-\bar{\tau}_o \pm \Delta)} &= \frac{1}{T_c}\int_0^{T_c} c_I(t-\tau_o)c_I(t-\bar{\tau}_o \pm \Delta)dt \\ &= R(\tau_o-\bar{\tau}_o \pm \Delta) = R(\tau \pm \Delta)\end{aligned} \quad (2\text{-}40)$$

the $\{K_i, i=1,2\}$ are the phase detector (multiplier) gain factors, which in general are not identical unless great care has been taken to balance the circuit design. The fact that K_1 and K_2 may not be identical in a practical situation is the reason why the noncoherent

DLL is sensitive to these gains. The waveforms $x_i(t)$ and $x_2(t)$ are envelope-detected and then squared. Considering the output of the discriminator in a noiseless environment, setting $N_i(t) = 0$ and substituting into Equation (2-38):

$$x_i(t) = \sqrt{2P}K_i R(\tau \pm \Delta)\cos\left(\omega_o t + \phi(t)\right) \quad i = 1,2 \qquad (2\text{-}41)$$

These waveforms are of the form [33]:

$$x_i(t) = Y_i(t)\cos\left(\omega_o t + \phi_i(t)\right), \quad i = 1,2 \qquad (2\text{-}42)$$

where

$$Y_i(t) = \sqrt{2P}K_i R(\tau \pm \Delta)$$

denotes the envelope of a signal waveform $\phi_i(t)$ denotes its phase. The difference of the early and late quadrature detector output becomes:

$$z_\Delta(\tau) = Y_2^2(t) - Y_1^2(t) \qquad (2\text{-}43)$$

$$z_\Delta(\tau) = 2P\left[K_2^2 R^2(\tau - \Delta) - K_1^2 R^2(\tau + \Delta)\right] \qquad (2\text{-}44)$$

For the ideal case when $K_1 = K_2$ assuming no arm imbalance, the error signal is written as:

$$z_\Delta(\tau) = K\left[R^2(\tau - \Delta) - R^2(\tau + \Delta)\right] \qquad (2\text{-}45)$$

$$K = 2PK_1^2 \qquad (2\text{-}46)$$

and the S-curve of noncoherent DLL is obtained to be proportional to:

$$G(\tau) = R^2(\tau - \Delta) - R^2(\tau + \Delta) \qquad (2\text{-}47)$$

Using the definition of the normalized chip timing error $\varepsilon = \frac{\tau}{T_c}$ and the early-late discriminator offset $\delta = \frac{\Delta}{T_c}$ Equation (2-47) above becomes:

$$G(\varepsilon) = R^2(\varepsilon - \delta) - R^2(\varepsilon + \delta) \qquad (2\text{-}48)$$

This is the discriminator S-curve for the noncoherent DLL and is used in analyzing the performance. The S-curve for the noncoherent DLL is shown in Figure (2-9) for the Rectangular pulse shape at early-late discriminator offset δ = 0.5 and 1.

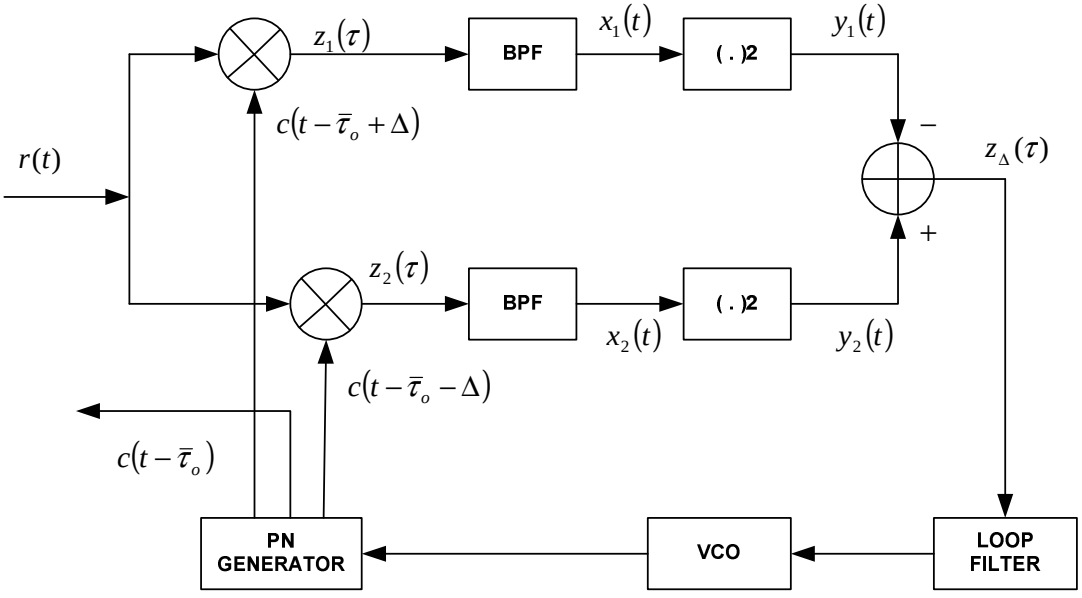

Figure 2-8 : Noncoherent delay lock tracking loop

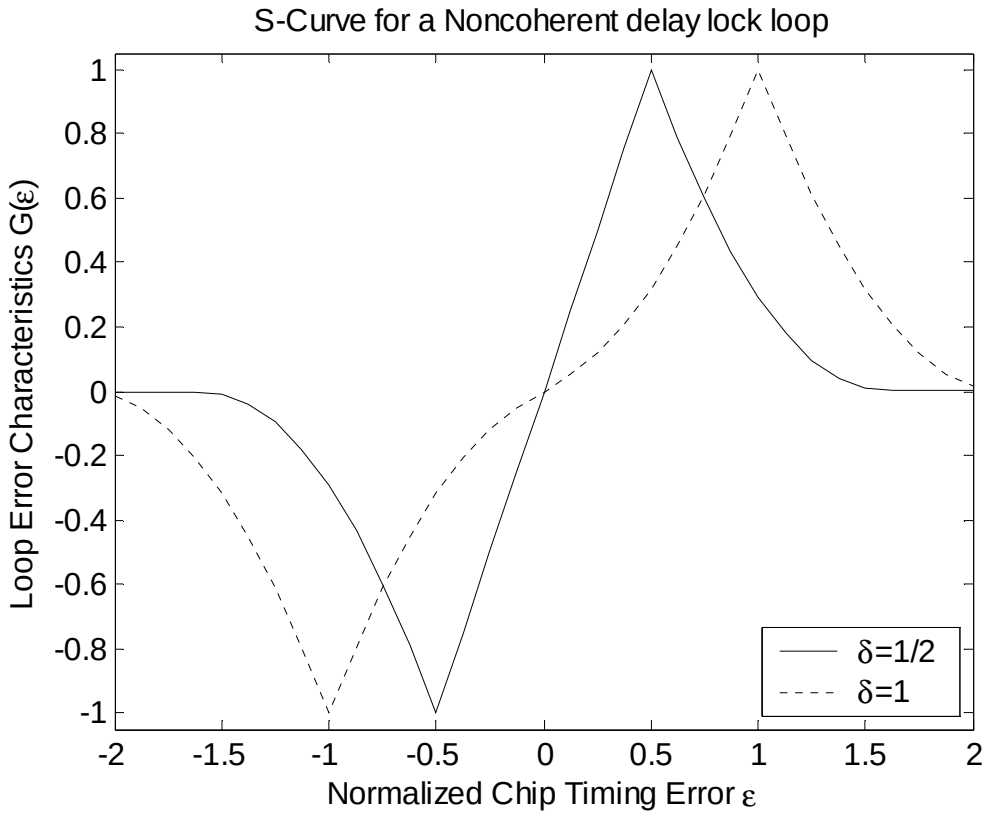

Figure 2-9 : Noncoherent DLL S-curve using Rectangular Pulse Shape

2.4 Summary

The CDMA system model has been presented in this chapter. The basis of the analysis of the code tracking loop, the digital phase lock loop linear model and the closed loop transfer function derived. The loop error characteristic equation for the Noncoherent delay lock loop has also been presented. The results from this section are used in our analysis of the performance of the Noncoherent DLL and to quantify the effect of pulse shaping on performance.

Chapter 3

Pulse Shaping for Noncoherent Delay Lock Loop

This chapter presents the measurement of the performance of the noncoherent delay lock loop (NCDLL) based on the linear model to derive the tracking jitter and on the nonlinear model to derive the mean-time-to-lose lock. The results from both are used to quantify the effect of pulse shaping on the loop. The effect of pulse shaping is experienced from two perspectives, the effect on the variance of the multiple access interference and the effect on the slope of the loop error characteristic at the origin. Numerical results are presented for different pulse shapes. The effects are also presented in the presence of

multiple users in the system. Finally the effect of varying the early-late discriminator offset with the tradeoff in mean-time-to lose lock is discussed.

3.1 Performance Measures

In order to quantify the effect of pulse shapes on the noncoherent DLL, the measure of performance of the tracking loop is first derived. Tracking performance can be measured in two ways using two theories – linear theory and nonlinear theory. Using the linear theory, the tracking jitter (root-mean-square tracking error) is evaluated while using the nonlinear theory the mean-time-to-lose lock (MTLL) is evaluated. The linear theory assumes high signal-to-noise ratio (SNR) while nonlinear analysis is found useful when the system operates at low SNR.

3.1.1 Tracking Jitter

Linear loop analysis is used to obtain the tracking jitter (RMS tracking error). At high SNR, the tracking error will usually be small enough such that the error measurement can be taken as a linear function of the relative timing error. The results obtained using linear loop analyses are considered to be good approximations of the actual performance at high SNR. More importance is given to the steady state tracking performance results obtained from the linear theory since in most situations the equivalent loop SNR is sufficiently high [7] as to justify this assumption. Given the mean of the timing error measurement

(Appendix A), the discriminator output can be defined as a normalized function of the relative timing error τ / T_c:

$$E[z_\Delta(\tau / T_c)] = N^2 E_c G(\tau / T_c) \qquad (3\text{-}1)$$

where for the Noncoherent DLL:

$$G(\tau / T_c) = R^2\left(\frac{\tau - \Delta}{T_c}\right) - R^2\left(\frac{\tau + \Delta}{T_c}\right) \qquad (3\text{-}2)$$

The time tracking model Figure (3-1) is obtained from the linear model of a digital phase lock loop in Figure (2-4) where the phase detector nonlinearity function G from Equation (3-1) is:

$$G = N^2 E_c G(\tau / T_c) \qquad (3\text{-}3)$$

The clock timing is maintained by a voltage controlled oscillator (VCO). The clock frequency of the VCO is controlled by the timing error measurement as scaled and filtered by the digital filter. The absolute timing on each chip is modified according to the sum of all frequency changes previously caused by timing errors. Hence the VCO timing (phase) is modeled by $z^{-1}/(1 - z^{-1})$, an accumulator over all previous corrections. Using the linear theory, the gain function $G(\tau / T_c)$ of the phase detector nonlinearity function G is replaced by its slope at $\tau = 0$:

$$G(\tau / T_c) \approx \left.\frac{dG(\tau / T_c)}{d(\tau / T_c)}\right|_{\tau=0} = \kappa \qquad (3\text{-}4)$$

The phase detector function becomes:

$$G = N^2 E_c \kappa \qquad (3\text{-}5)$$

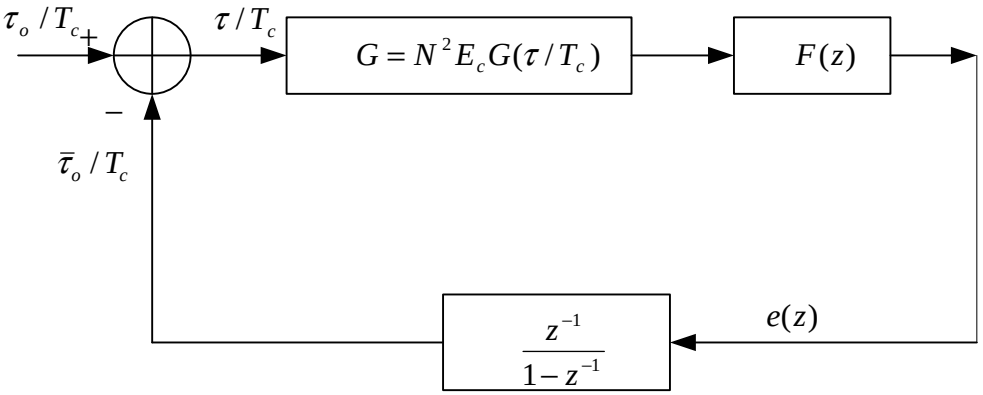

Figure 3-1 : Time Tracking Loop Model

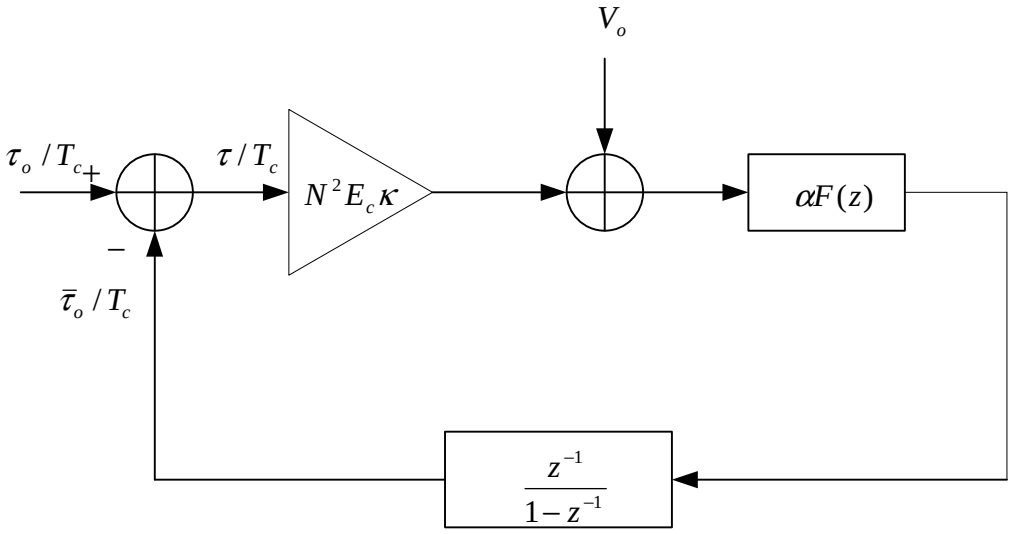

Figure 3-2 : Linear Model of Time Tracking Loop

The digital filter $F(z)$ is replaced by $\alpha F(z)$ where the scale factor α represents the gain introduced in the voltage-to-frequency conversion. The linear model of the time tracking loop is formulated taking into consideration these changes. The timing error measurement from Equation (2-13) is:

$$\frac{\tau(z)}{T_c} = \frac{(z-1)}{(z-1)+N^2 E_c \kappa\alpha F(z)} \frac{\tau_o}{T_c} \tag{3-6}$$

$$\frac{\tau(z)}{T_c} = [1-H(z)] \frac{\tau_o}{T_c} \tag{3-7}$$

where $H(z)$ is the closed loop transfer function. From Equation (2-17):

$$H(z) = \frac{N^2 E_c \kappa\alpha F(z)}{(z-1)+N^2 E_c \kappa\alpha F(z)} \tag{3-8}$$

The generating function for the timing error due to an initial relative delay τ_o / T_c is represented by a step function $(1/1-z^{-1})$, from Equation (2-15):

$$\frac{\tau(z)}{T_c} = \frac{\tau_o}{T_c}[1-H(z)]\left(\frac{1}{1-z^{-1}}\right) \tag{3-9}$$

$$\frac{\tau(z)}{T_c} = \frac{\tau_o}{T_c}\left[\frac{z-1}{(z-1)+N^2 E_c \kappa\alpha F(z)}\right]\left(\frac{z}{z-1}\right) \tag{3-10}$$

$$\frac{\tau(z)}{T_c} = \frac{\tau_o}{T_c}\left[\frac{z}{(z-1)+N^2 E_c \kappa\alpha F(z)z^{-1}}\right] \tag{3-11}$$

$$\frac{\tau(z)}{T_c} = \frac{\tau_o}{T_c}\left[\frac{1}{1-z^{-1}+N^2 E_c \kappa\alpha F(z)z^{-1}}\right] \tag{3-12}$$

If the digital filter $F(z)=1$, the tracking loop is first order so Equation (3-12) becomes:

$$\frac{\tau(z)}{T_c} = \frac{\tau_o}{T_c}\left[\frac{1}{1 - z^{-1} + N^2 E_c\, \kappa\alpha\, z^{-1}}\right] \qquad (3\text{-}13)$$

This requires for stability α to be:

$$\alpha < 1/(\kappa N^2 E_c) \qquad (3\text{-}14)$$

The smaller the value of α the more slowly the error decays. From Equation (3-13), the variance of the timing error is given by [2]:

$$Var(\tau / T_c) = \frac{V_o}{(N^2 E_c \kappa)^2} B_L \qquad (3\text{-}15)$$

where B_L is the loop bandwidth defined as:

$$B_L = \oint_c H(z) H(z^{-1}) \frac{dz}{j2\pi z} \qquad (3\text{-}16)$$

c denotes the contour of integration and V_o is the total interference variance from Appendix A as:

$$V_o = Var[z_\Delta(\tau)] \le 2(NI_o)^2 \left[1 + 2N(E_c / I_o)\right] \qquad (3\text{-}17)$$

I_o is the variance of the interference due to other users. Integrating B_L around a unit circle with V_o bounded by Equation (3-17) and α by Equation (3-14), Equation (3-15) becomes [2]:

$$Var(\tau / T_c) < \frac{2I_o^2 \alpha + 4NI_o E_c \alpha}{E_c \kappa} \qquad (3\text{-}18)$$

By observing that I_o^2 is the dominant term [34] in the denominator because the energy per chip E_c is small compared to I_o, the variance of the timing error is approximated by [34]:

$$Var(\tau / T_c) \approx \frac{2I_o^2 \alpha}{E_c \kappa} \qquad (3\text{-}19)$$

We desire the tracking loop to converge as quickly as possible without making the loop become unstable. We use the approximation $\alpha \approx 1/(N^2 E_c \kappa)$ to be as close as possible for the swiftest decay without actually being equal. The variance is further approximated to:

$$Var(\tau / T_c) \approx \frac{2I_o^2}{N^2 E_c^2 \kappa^2} \qquad (3\text{-}20)$$

From here the RMS tracking error σ becomes:

$$\sigma \approx \frac{\sqrt{2} I_o}{N E_c \kappa} \qquad (3\text{-}21)$$

This performance equation will be used in measuring the effect of varying the pulse shape on the noncoherent delay lock loop.

3.1.2 Mean-Time-To-Lose Lock

Nonlinear analysis is useful when the system operates at low SNR. In these situations the mean-time-to-lose lock (MTTL) is of primary consideration. The ability of the code tracking loop to maintain lock is an important consideration in assessing the overall performance of a spread spectrum receiver. One measure of this ability is the probability of remaining in lock for a given interval of time. Unfortunately, analytical evaluation of

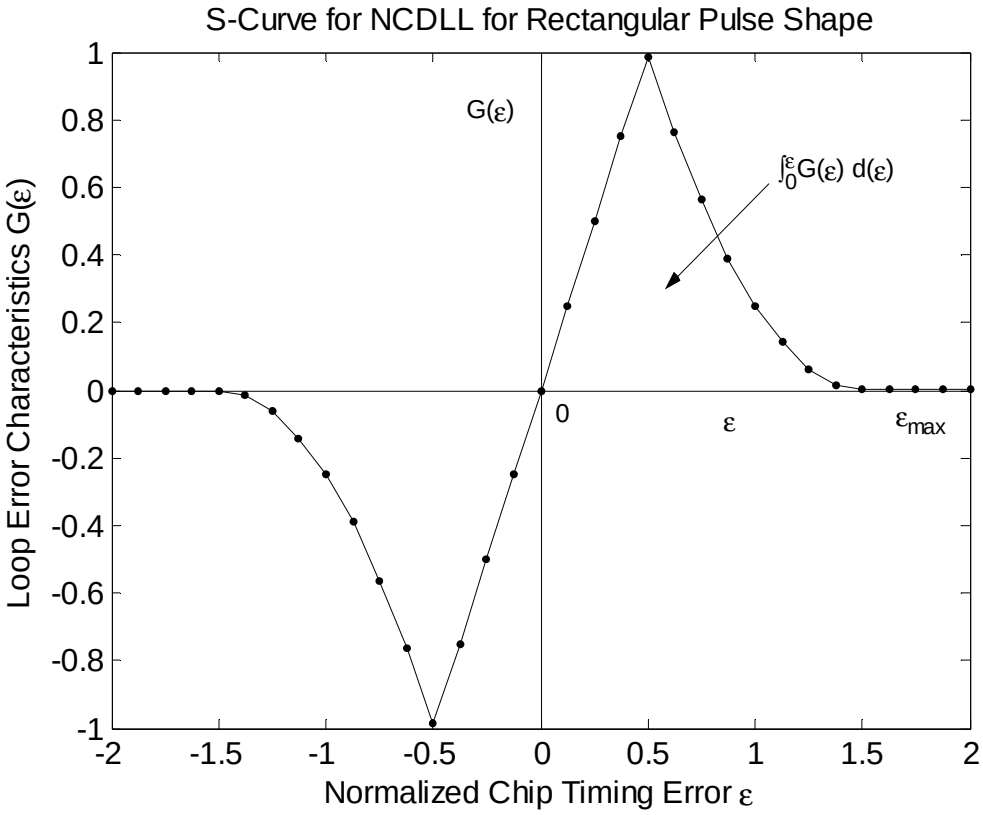

Figure 3-3 : S-curve of NCDLL showing the Boundary

this measure is difficult [7] and thus an alternate measure used is the mean time to lose lock. The MTTL is defined as the time taken for the timing error ε to reach a chosen boundary $\varepsilon_{\max}$. Figure (3-3) shows the loop error characteristic of the Noncoherent DLL showing the boundary $\varepsilon_{\max}$. The MTTL is a special case of the more general problem of finding the n^{th} moment of the first passage time of the error process in a synchronous control system [7] . The solutions to the problems of this nature are typically obtained by assuming that the noise process driving the system is wideband compared to the system bandwidth, in which case the error process can be assumed to be Markovian and its probability density function a solution to the Fokker-Planck equation [17].

By applying the boundary condition to the time-dependent solution of the one-dimensional Fokker-Plank equation, the first moment of the passage of time of the error process in a first order synchronous control system with symmetrical boundaries $\pm b$ and symmetrical restoring force $f_{res}(x)$ is given by [35]:

$$T = \frac{1}{K}\int_0^b\int_0^b \exp[U(y)-U(x)]dy\,dx \qquad (3\text{-}22)$$

where $U(x)$ is the system potential function which is related to the restoring force $f_{res}(x)$ as:

$$U(x) = \int^x f_{res}(y)dy \qquad (3\text{-}23)$$

and K is the second-order intensity coefficient in the Fokker-Plank equation. Applying this to the noncoherent delay lock loop, the mean time to lose lock as a function of the variance and loop bandwidth is given by [36] :

$$T = \frac{1}{4B_L\sigma^2}\int_0^{\varepsilon_{\max}}\int_{\varepsilon}^{\varepsilon_{\max}} \exp\left[U(\varepsilon') - U(\varepsilon)\right] d\varepsilon' \, d\varepsilon \qquad (3\text{-}24)$$

where σ^2 is the noise variance, B_L is the loop bandwidth. The system potential function $U(\varepsilon)$ is the minimum escape energy [37] and is related to the area under the S-curve Figure (3-3). $U(\varepsilon)$ is given by [36]:

$$U(\varepsilon) = \frac{1}{\sigma^2}\int_0^{\varepsilon_{\max}} G(\varepsilon)\, d\varepsilon \qquad (3\text{-}25)$$

$G(\varepsilon)$ is the discriminator S-curve for the delay lock loop. Normalizing by the loop bandwidth Equation (3-24) becomes:

$$B_L T = \frac{1}{4\sigma^2}\int_0^{\varepsilon_{\max}}\int_{\varepsilon}^{\varepsilon_{\max}} \exp\left[U(\varepsilon') - U(\varepsilon)\right] d\varepsilon' \, d\varepsilon \qquad (3\text{-}26)$$

The derived expression for the MTTL is used in determining the tradeoff occurring between the variance and the MTTL from using different NCDLL early-late discriminator offset for different pulse shapes.

3.2 Impact of Pulse Shaping

In our analysis of the impact of pulse shaping, the frequency domain formulation is used because it simplifies the problem at hand. The RMS tracking error σ in Equation (3-21) is seen to directly relate to I_o, the multiple-access interference variance and inversely relate to κ, the slope of the NCDLL at the origin.

The interference caused by other users sharing the band of user k is not white, since they are all assumed to use the same spectral shaping filter. However, there will be other users in the contiguous bands, so the composite of all other users' signals in all bands may be taken to be essentially Gaussian noise with uniform spectral density [2].

The multiple-access interference variance I_o due to the other $k-1$ interfering users is given by [2]:

$$I_o = \sum_{j \neq k} E_c(j) \int_{-\infty}^{+\infty} |H(f)|^4 df / T_c \qquad (3\text{-}27)$$

where $H(f)$ is the Fourier transform of the chip waveform $h(t)$. Suppose we normalize the chip energy to be equal for all pulse shapes and assume perfect power control, so that all users are received by the base station receiver at the same power or chip energy level E_c, the multiple-access interference variance reduces to:

$$I_o = \int_{-\infty}^{+\infty} |H(f)|^4 df \qquad (3\text{-}28)$$

The slope κ for the NCDLL is evaluated from the differential of the gain function $G(\varepsilon)$. The S-curve of the noncoherent DLL as a normalized function of the relative timing error ε from Equation (2-48) is $G(\varepsilon) = R^2(\varepsilon - \delta) - R^2(\varepsilon + \delta)$. For constant-envelope phase modulation of interest, the complex autocorrelation is real [8], $R^2(\varepsilon \pm \delta)$ is therefore replaced by $4|R(\varepsilon \pm \delta)|^2$ and Equation (2-48) becomes:

$$G(\varepsilon) = 4[|R(\varepsilon - \delta)|^2 - |R(\varepsilon + \delta)|^2] \qquad (3\text{-}29)$$

The slope κ of the S-curve evaluated at $\tau = 0$:

$$\kappa = \left.\frac{dG(\tau / T_c)}{d(\tau / T_c)}\right|_{\tau=0} = \left.\frac{dG(\varepsilon)}{d(\varepsilon)}\right|_{\varepsilon=0} = 8[R'(\varepsilon - \delta)R(\varepsilon - \delta) - R'(\varepsilon + \delta)R(\varepsilon + \delta)] \qquad (3\text{-}30)$$

$$\kappa = 8[R'(-\delta)R(-\delta) - R'(\delta)R(\delta)] \qquad (3\text{-}31)$$

For long PN codes modeled as a random signature sequence, the frequency domain representation of autocorrelation function R reduces to:

$$R(\delta) = \int_{-\infty}^{+\infty} |H(f)|^2 \cos(2\pi f\delta)\,df \qquad (3\text{-}32)$$

$R(\delta)$ is an even function hence:

$$R(-\delta) = \int_{-\infty}^{+\infty} |H(f)|^2 \cos(-2\pi f\delta)\,df = \int_{-\infty}^{+\infty} |H(f)|^2 \cos(2\pi f\delta)\,df$$

$$\textit{therefore} \quad R(\delta) = R(-\delta) \qquad (3\text{-}33)$$

Similarly $R'(\delta)$ is an odd function hence:

$$R'(\delta) = \int_{-\infty}^{+\infty} -2\pi f |H(f)|^2 \sin(2\pi f\delta)\,df \quad \text{and} \quad R'(-\delta) = \int_{-\infty}^{+\infty} 2\pi f |H(f)|^2 \sin(2\pi f\delta)\,df$$

$$therefore \quad -R'(\delta) = R'(-\delta) \tag{3-34}$$

Substituting (3-33) and (3-34) into (3-31) the slope κ becomes:

$$\kappa = 16R(\delta)R'(-\delta) \tag{3-35}$$

$$\kappa = 16\left[\int_{-\infty}^{+\infty} |H(f)|^2 \cos(2\pi f\delta)df\right]\left[\int_{-\infty}^{+\infty} 2\pi f |H(f)|^2 \sin(2\pi f\delta)df\right] \tag{3-36}$$

With the frequency domain formulation for I_o and κ we go ahead to show the impact of pulse shape $h(t)$ on the RMS tracking jitter σ.

3.3 Numerical and Simulation Results

Full-response pulse shapes confined to single chip interval are considered. Inter-chip interference introduced by the pulse shape is therefore neglected since CDMA is dominated by multiple access interference. The pulse shapes having the following functions are considered:

$$\text{Rectangular } h(t) = \begin{cases} 1, & 0 \le t < T_c \\ 0, & otherwise \end{cases}; \tag{3-37}$$

$$\text{Triangular } h(t) = \begin{cases} 1 - \left|\frac{2t}{T_c} - 1\right|, & 0 \le t < T_c \\ 0, & otherwise \end{cases}; \tag{3-38}$$

$$\text{Half Sine } h(t) = \begin{cases} \sin\left(\frac{\pi t}{T_c}\right), & 0 \le t < T_c \\ 0, & otherwise \end{cases}; \tag{3-39}$$

$$\text{Raised Cosine}\, h(t) = \begin{cases} \frac{1}{2}\left(1 - \cos\frac{2\pi t}{T_c}\right), & 0 \le t < T_c \\ 0, & otherwise \end{cases}; \qquad (3\text{-}40)$$

$$\text{Hamming}\, h(t) = \begin{cases} 0.54 - 0.46\cos\left(\frac{2\pi t}{T_c}\right), & 0 \le t < T_c \\ 0, & otherwise \end{cases}; \qquad (3\text{-}41)$$

The pulse shapes with normalized energy are shown in Figure (3-4)-(3-8). Table (3-1) shows the factor used to normalize the different pulse shapes to have equal energy.

Table 3-1 : Normalization Factor for Different Pulse Shape

PULSE SHAPE	FACTOR
Rectangular	1
Triangular	$\sqrt{3}$
Half-Sine	$\sqrt{2}$
Raised-Cosine	$\sqrt{8/3}$
Hamming	$\sqrt{2.516}$

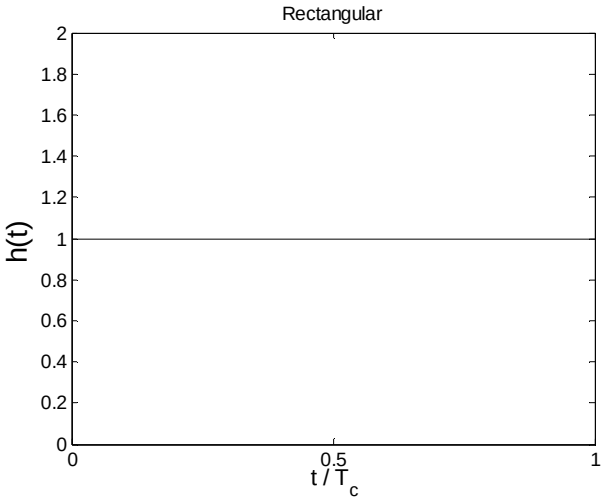

$$\text{Rectangular } h(t) = \begin{cases} 1, & 0 \le t < T_c \\ 0, & otherwise \end{cases}$$

Figure 3-4 : Rectangular Pulse Shape

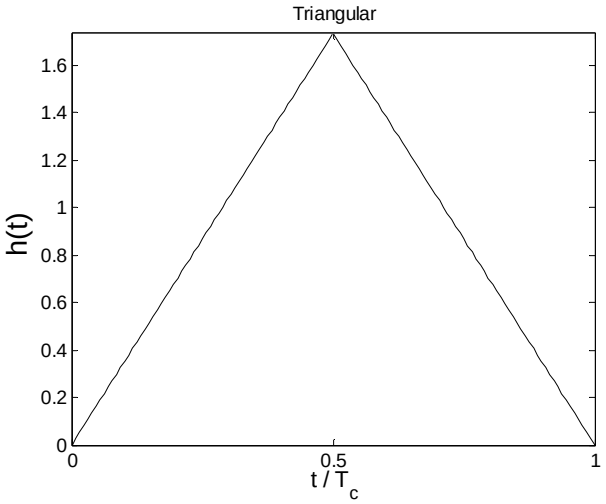

$$\text{Triangular } h(t) = \begin{cases} 1 - \left| \frac{2t}{T_c} - 1 \right|, & 0 \le t < T_c \\ 0, & otherwise \end{cases}$$

Figure 3-5 : Triangular Pulse Shape

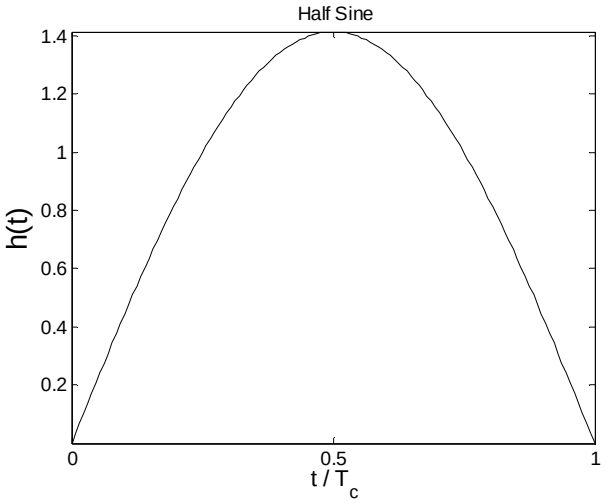

$$\text{Half Sine}\, h(t) = \begin{cases} \sin\left(\dfrac{\pi t}{T_c}\right), & 0 \le t < T_c \\ 0, & otherwise \end{cases}$$

Figure 3-6 : Half Sine Pulse Shape

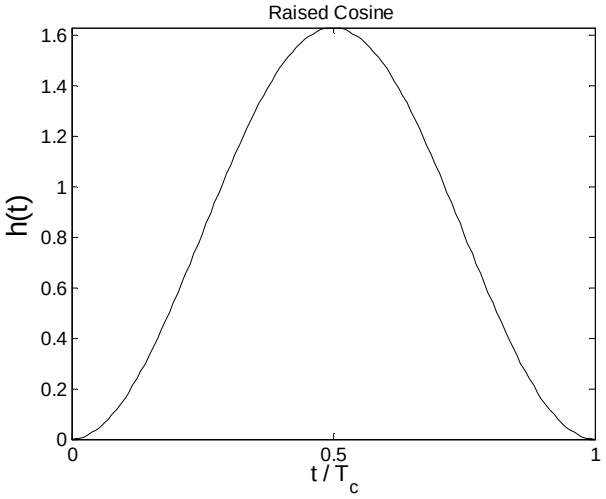

$$\text{Raised Cosine}\, h(t) = \begin{cases} \dfrac{1}{2}\left(1 - \cos\dfrac{2\pi t}{T_c}\right), & 0 \le t < T_c \\ 0, & otherwise \end{cases};$$

Figure 3-7 : Raised Cosine Pulse Shape

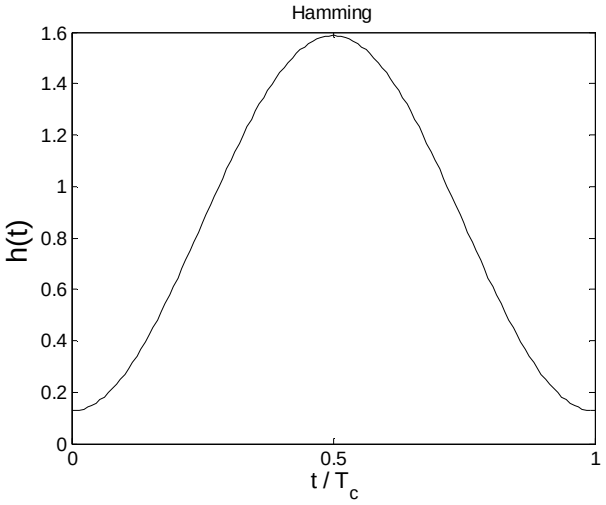

$$\text{Hamming } h(t) = \begin{cases} 0.54 - 0.46\cos\left(\dfrac{2\pi t}{T_c}\right), & 0 \le t < T_c \\ 0, & otherwise \end{cases}$$

Figure 3-8 : Hamming Pulse Shape

3.3.1 Discussion

With an early-late discriminator offset $\delta = 0.5$, the loop error characteristic S-curve $G(\varepsilon)$ for the different pulse shapes considered is plotted against the normalized chip timing error ε. Each pulse shape exhibit different S-curve as shown in Figure (3-9). A closer look at the slopes of the S-curves at the origin in Figure (3-10) shows clearly the different slopes for each pulse shape at the origin. The multiple-access interference variance I_o from Equation (3-28) is evaluated by taking the Fourier transforms and numerical integral of the pulse shapes. The multiple-access interference variance is tabulated in Table (3-2). The derived slope κ at the origin Equation (3-36) is also evaluated for an early-late discriminator offset $\delta = 0.5$ and tabulated in Table (3-3). The derived expression for κ is observed to accurately quantify the slopes at the origin of the loop error characteristic S-curve Figure (3-10). Since the performance of the NCDLL Equation (3-21) is inversely related to the slope at the origin κ, it can be inferred that the pulse shapes with the least slope at the origin will have the greatest RMS tracking error and hence the least performance.

The least slope belongs to the Raised-Cosine pulse shape. The next is the Hamming and the Triangular in that order. The position for the greatest slope is shared both by the Rectangular pulse shape and the Half-Sine. Their respective performances' is observed to follow the same trend as their slopes. Simulated performance in additive white Gaussian noise channel (AWGN) is shown in Figure (3-11). The slightly better performance exhibited by the Half-Sine when compared to the Rectangular is due to its lower

multiple-access interference variance I_o. The effect of this multiple access interference will be seen to be more pronounced as the number of users increase.

TABLE 3-2: MULTIPLE-ACCESS INTERFERENCE VARIANCE

PULSE SHAPE	I_o
Raised-Cosine	0.24055
Hamming	0.26368
Triangular	0.26964
Rectangular	0.33333
Half-Sine	0.29332

TABLE 3-3 : SLOPE AT THE ORIGIN ($\delta = 0.5$)

PULSE SHAPE	κ
Raised Cosine	0.889
Hamming	1.357
Triangular	1.500
Rectangular	2.000
Half-Sine	2.000

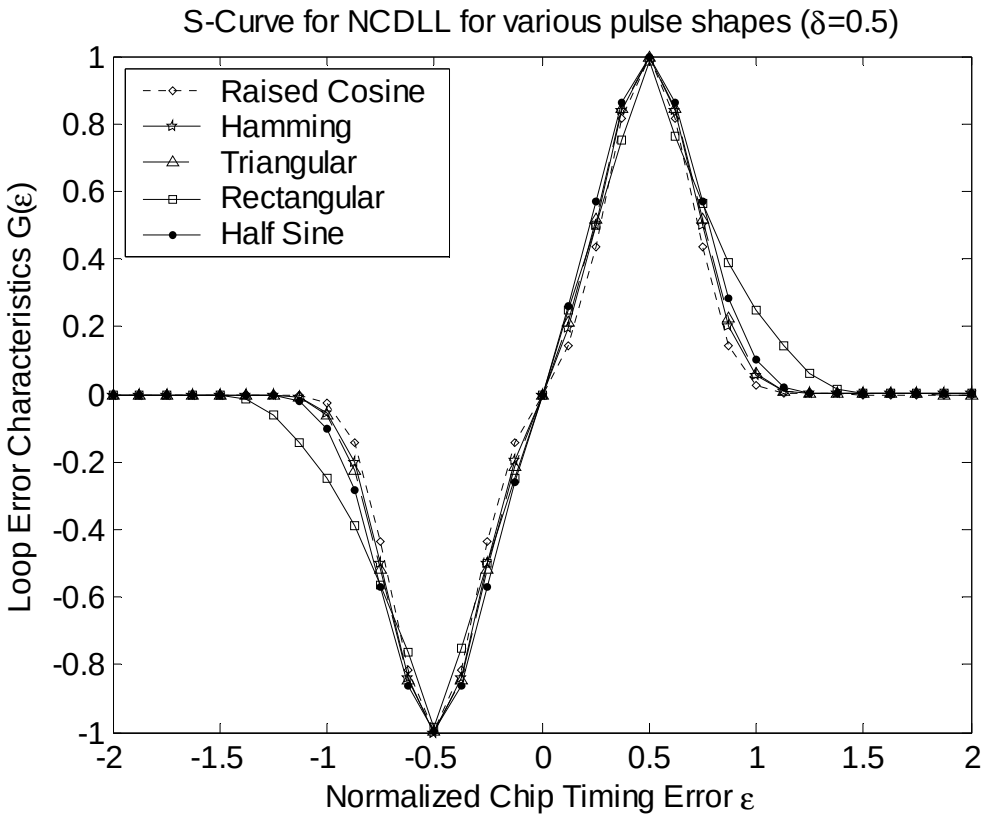

Figure 3-9 : S-curve for Noncoherent DLL for Various Pulse Shapes at 0.5 Early-Late Discriminator Offset

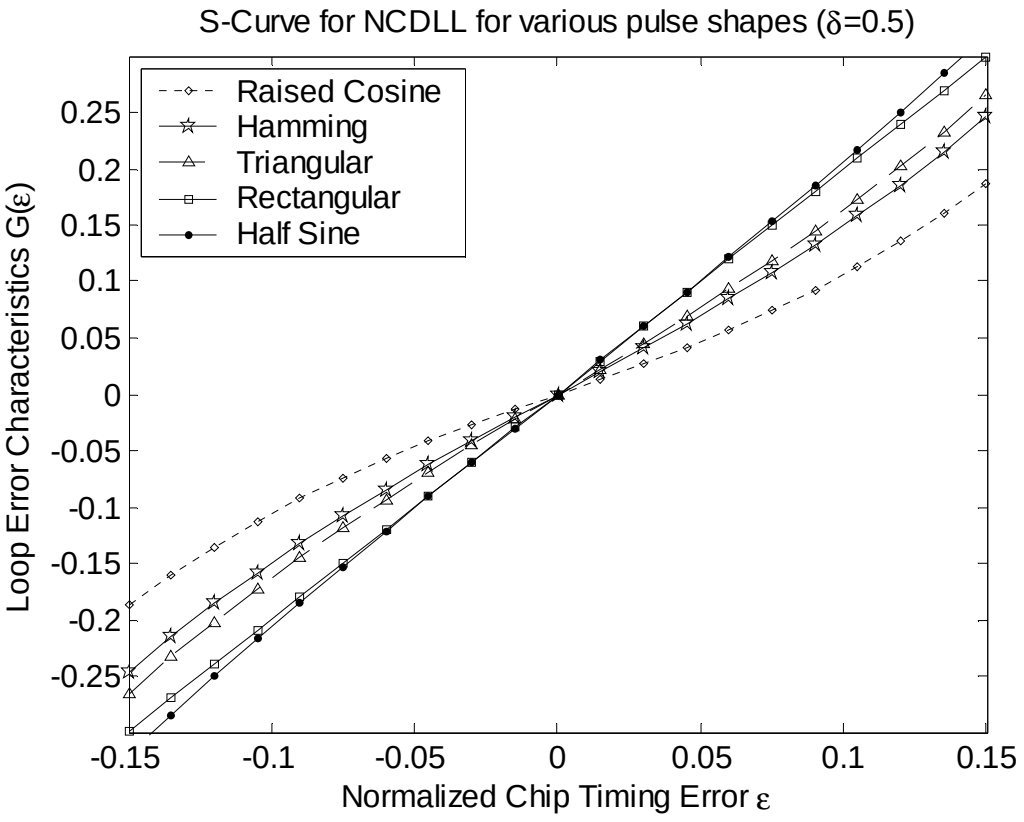

Figure 3-10 : S-curve for Noncoherent DLL for Various Pulse Shapes at the Origin for 0.5 Early-Late Discriminator Offset

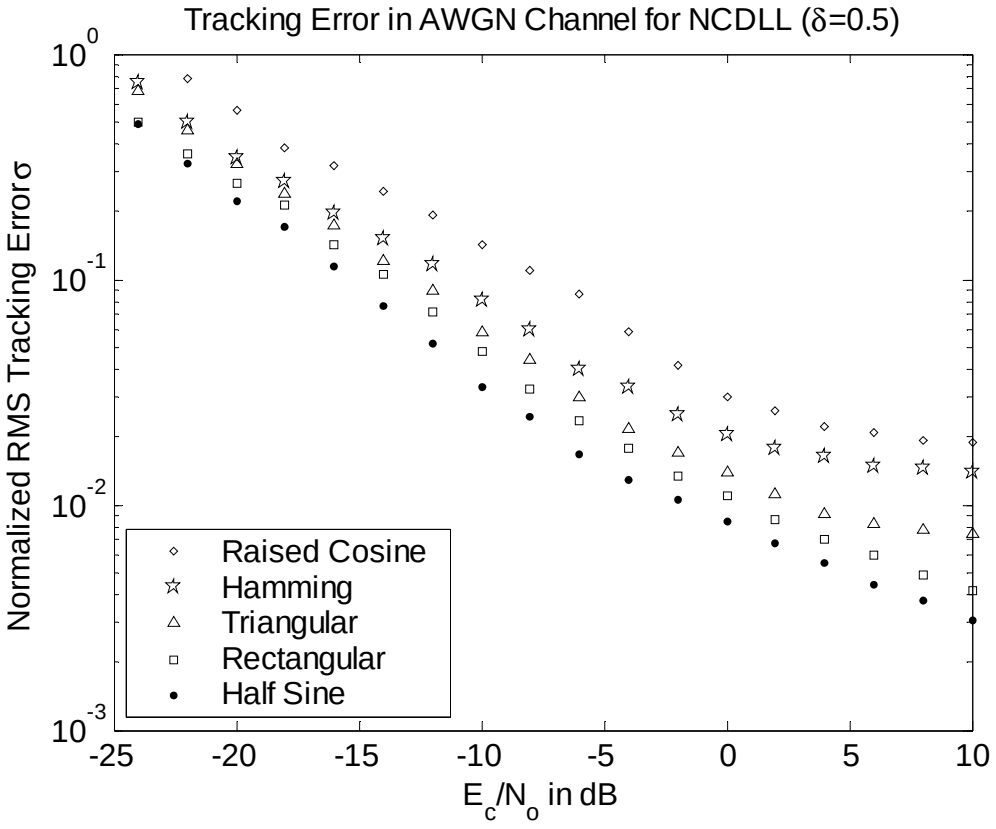

Figure 3-11 : Normalized RMS Tracking Error in AWGN Channel for NCDLL at 0.5 Early-Late Discriminator Offset

The analyses of the performance of the DLL all assume the additive white Gaussian channel (AWGN) [12, 13, 15, 17, 36]. For the simulated performance of various pulse shapes in the AWGN shown in Figure (3-11), the Half-sine pulse shape exhibit the best performance with lowest RMS tracking error while the Raised-Cosine pulse performs the worse. All other pulse shapes maintain the same inverse order as their respective slope κ at the origin.

A two-ray Rayleigh fading channel is also considered while investigating the effect of pulse shaping on the tracking performance of the noncoherent delay lock loop. The two-ray Rayleigh fading channel is well known to be a good model for urban cellular channels [23]. It is expected that with fading introduced, there would be performance degradation with an increase in the RMS tracking error for all the pulse shapes however the objective of introducing the channel is to observe if the degradation in performance will affect each pulse shape differently enough to cause a change in their performance relative to each other. When transmitting through a two-ray Rayleigh fading channel, the received signal from Equation (2-32) becomes [23]:

$$\begin{aligned} r(t) = \sqrt{2P}\{\ & \beta_1\ c(t-\tau_1)d(t-\tau_1)\cos(\omega_o t + \phi_1(t)) \\ & + \beta_2\ c(t-\tau_2)d(t-\tau_2)\cos(\omega_o t + \phi_2(t))\ \} + n(t) \end{aligned} \tag{3-42}$$

where $\tau_1 - \tau_2$ is the delay difference between the first and the second path. β_1 and β_2 are attenuation factors for each of the path of the fading channel which vary randomly according to the Rayleigh distribution. Without loss of generality, the first path can be considered to be the main path to be tracked by the code tracking loop. The simulated performance in the Rayleigh channel is shown in Figure (3-12).

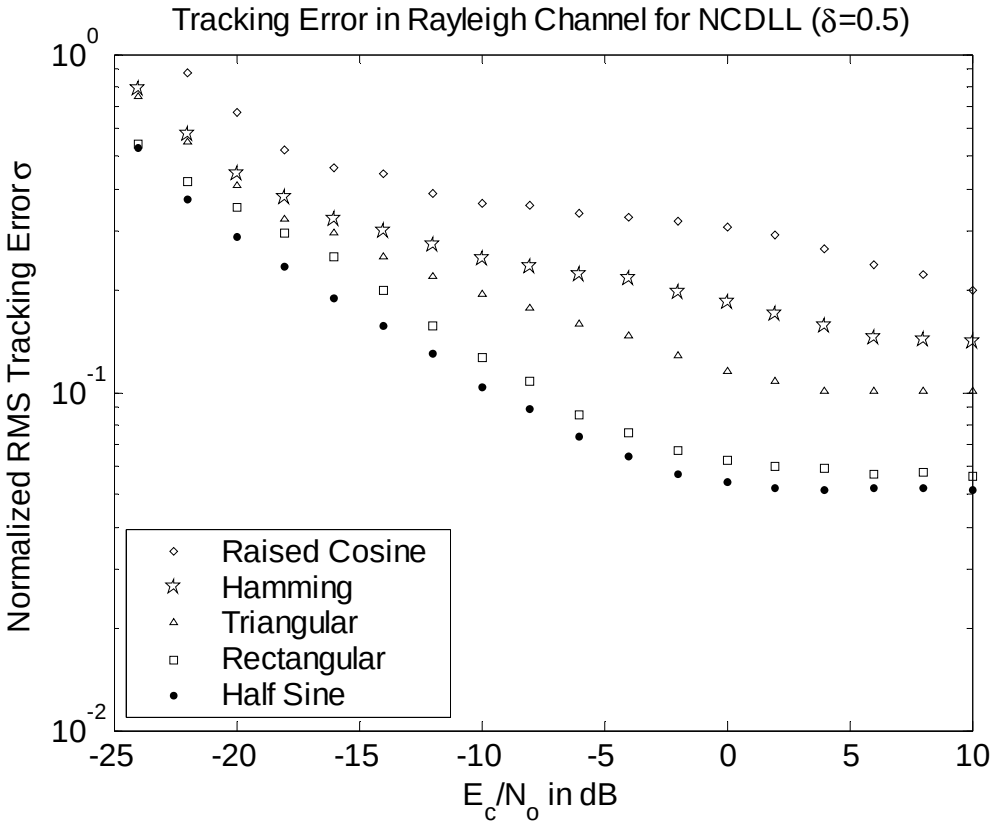

Figure 3-12 : Normalized RMS Tracking Error in Rayleigh Channel for NCDLL at 0.5 Early-Late Discriminator Offset

It is observed that the relative performance of one pulse shape compared to the others remain essentially unchanged when compared to their performance in an AWGN channel, notwithstanding the fading introduced.

The performance of the various pulse shapes in the presence of multiple users at a typical operating noise level $E_c / N_o = -10\,dB$ is shown in Figure (3-13). The normalized RMS tracking error is seen to increase approximately linearly as the number of users increase. It is observed that as the number of users increases, the variation between the respective performances of the pulse shapes also increase. This is due to the different multiple access interference variances of different pulse shapes. A difference of 25% in the normalized RMS tracking error is seen between the Raised Cosine and the Half Sine pulse shape when 5 users are in the system. This difference increases to 37% with 25 users.

The effect of different pulse shapes is better observed by taking fixed RMS tracking error. Table (3-4) shows the number of users supported by the system at a normalized RMS tracking error of 0.15. The best performing pulse shape – the Half Sine pulse shape is able to support 11 times more users than the worse performing pulse shape - the Raised Cosine. The system is hereby observed to be able to accommodate a larger number of users at any given error level with better pulse shapes.

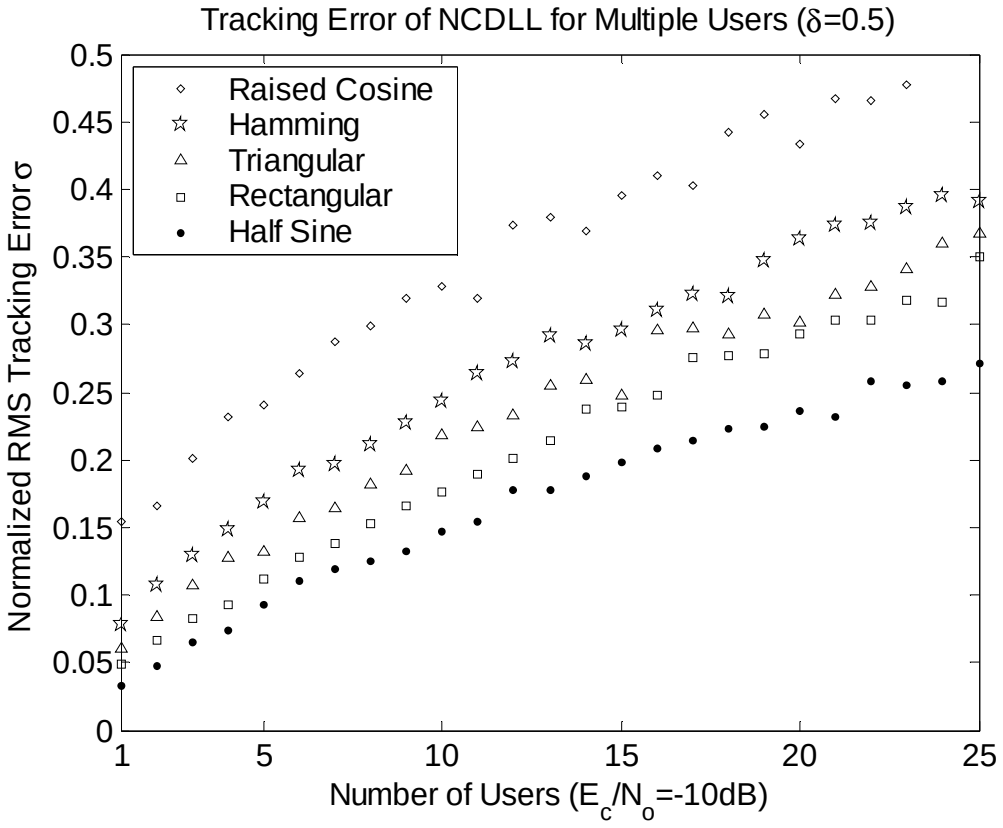

Figure 3-13 : Normalized RMS Tracking Error for Multiple Users at 0.5 Early-Late Discriminator Offset

TABLE 3-4 : NUMBER OF USERS MAINTAINED AT σ = 0.15 FOR δ = 0.5

PULSE SHAPE	NO OF USERS
Raised Cosine	1
Hamming	4
Triangular	6
Rectangular	8
Half-Sine	11

3.4 Arbitrary Early-Late Discriminator Offset

We have considered the assumption up till this point of an early-late discriminator offset $\delta = 0.5$. Changing the early-late discriminator offset for the NCDLL however has an interesting effect on its slope at the origin κ and hence on its performance. Figure (3-14) shows the loop error characteristic S-curve for the Rectangular pulse shape for different early-late discriminator offset ($\delta = 0.1 - 0.9$). The slope at the origin decreases as the discriminator offset is increased. Theoretically the slope of the Rectangular pulse shape varies linearly as $\kappa = 4(1-\delta)$ [2]. The slopes of the other pulse shapes however do not follow a linear pattern. The slope κ is shown against different early-late discriminator offset for all considered pulse shapes in Figure (3-15).

It is observed that reducing the discriminator offset to less than 0.5 increases the slopes of all the pulse shapes and hence increases their respective performances. It is also worthy to note that decreasing the offset to less than 0.4 makes all other nonrectangular pulse shapes have a greater slope when compared to the Rectangular pulse shape and hence better performance. From Figure (3-15), Table (3-5) shows the range of early-late discriminator offset for other pulse shapes that guarantees a slope greater than the Rectangular pulse shape.

As an example, the NCDLL spacing is reduced to 0.4 making all other pulse shapes exhibit superior performance compared to the rectangular. The simulation of the performance of the NCDLL in AWGN channel at a spacing of 0.4 is shown in Figure (3-

16) confirming this expectation. Their performance in the presence of multiple users is shown in Figure (3-17). Apart from the observed superior performance of all the other pulse shapes compared to the Rectangular, there is a general decrease in the overall RMS tracking error for any particular number of users for all the pulse shapes when compared to their RMS tracking error at an early-late spacing of 0.5 in Figure (3-13). Table (3-6) shows the number of users supported by the system at a normalized RMS tracking error of 0.15. The best performing pulse shape – the Half Sine pulse shape is able to support 10 more users than the worse performing pulse shape - the Rectangular.

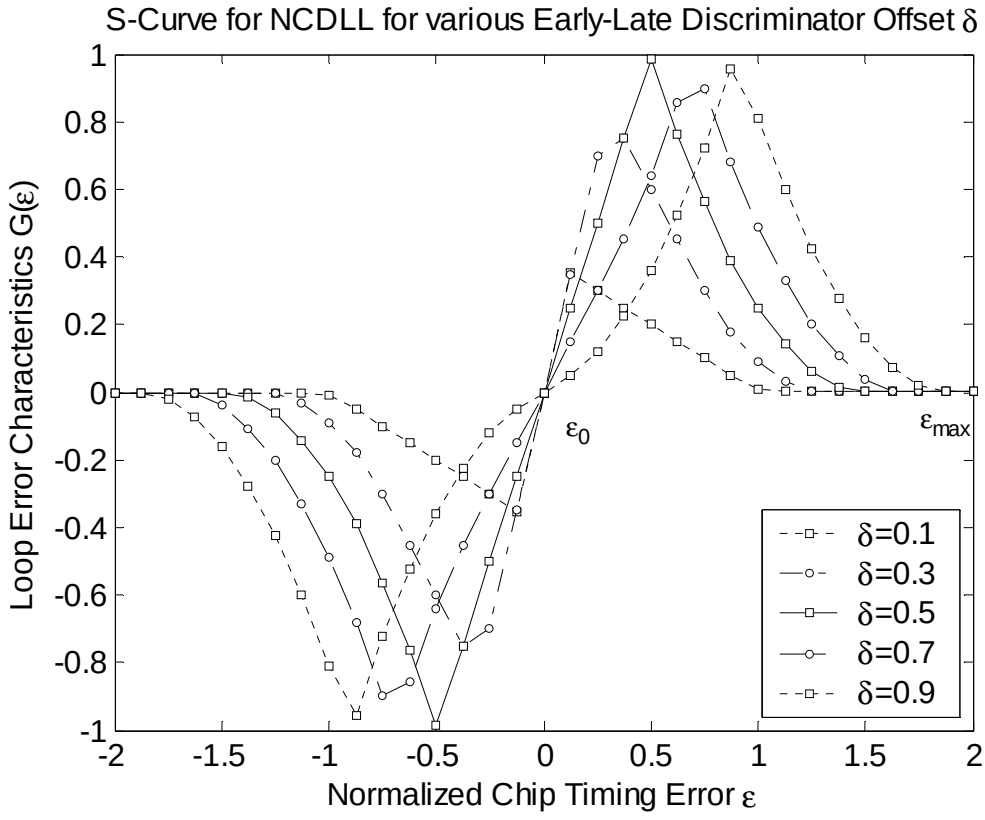

Figure 3-14 : S-curve for the NCDLL for various Early-Late Discriminator Offsets using the Rectangular Pulse Shape

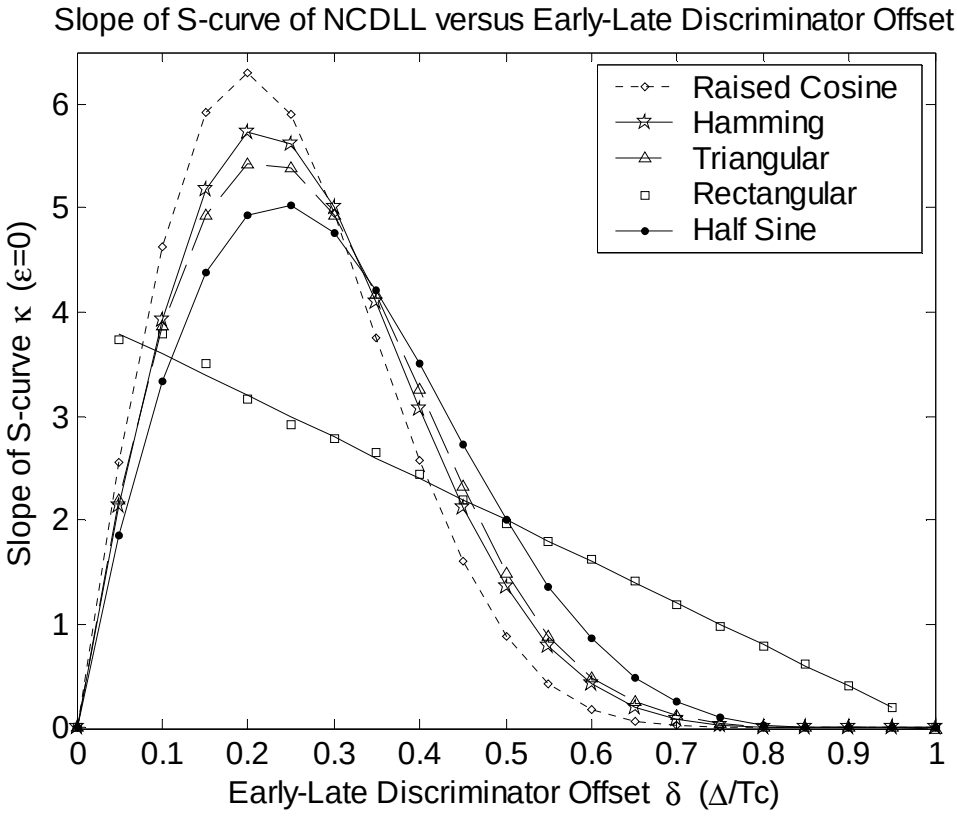

Figure 3-15 : Slope of S-curve of Noncoherent DLL versus Early-Late Discriminator Offset

TABLE 3-5 : RANGE WHERE THE SLOPE IS GREATER THAN THE RECTANGULAR

PULSE SHAPE	MIN	MAX
Raised-Cosine	0.077	0.411
Hamming	0.091	0.445
Triangular	0.093	0.460
Half-Sine	0.110	0.500

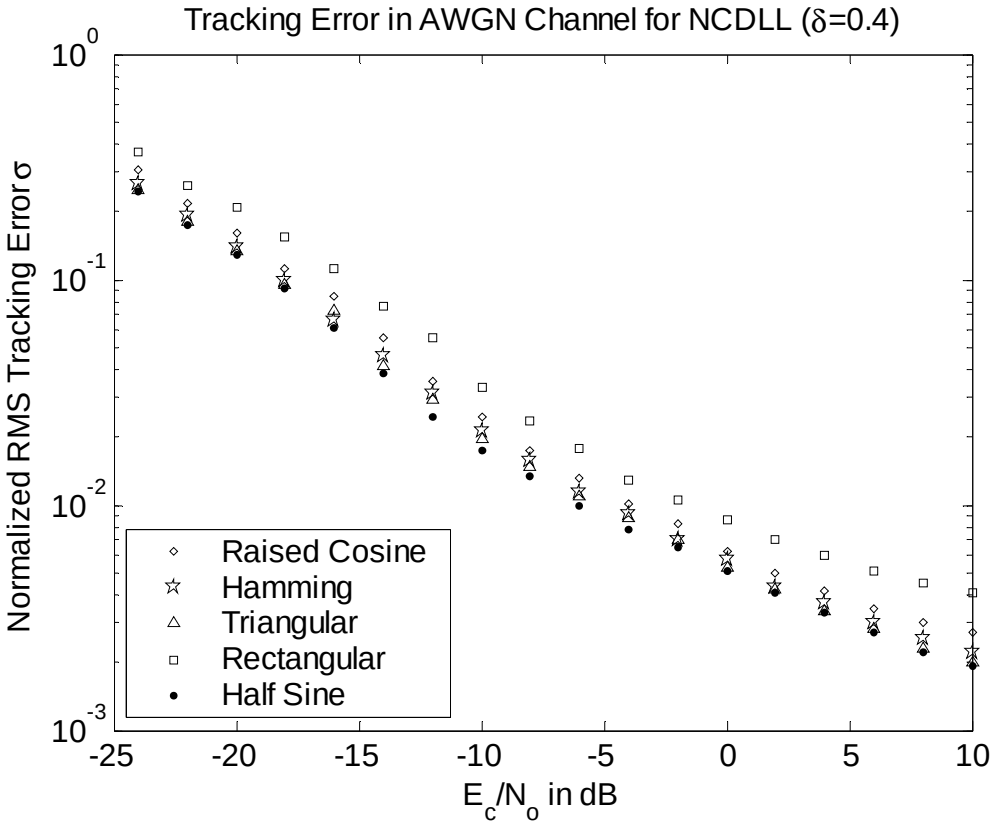

Figure 3-16 : Normalized RMS Tracking Error for NCDLL at 0.4 Early-Late Discriminator Offset

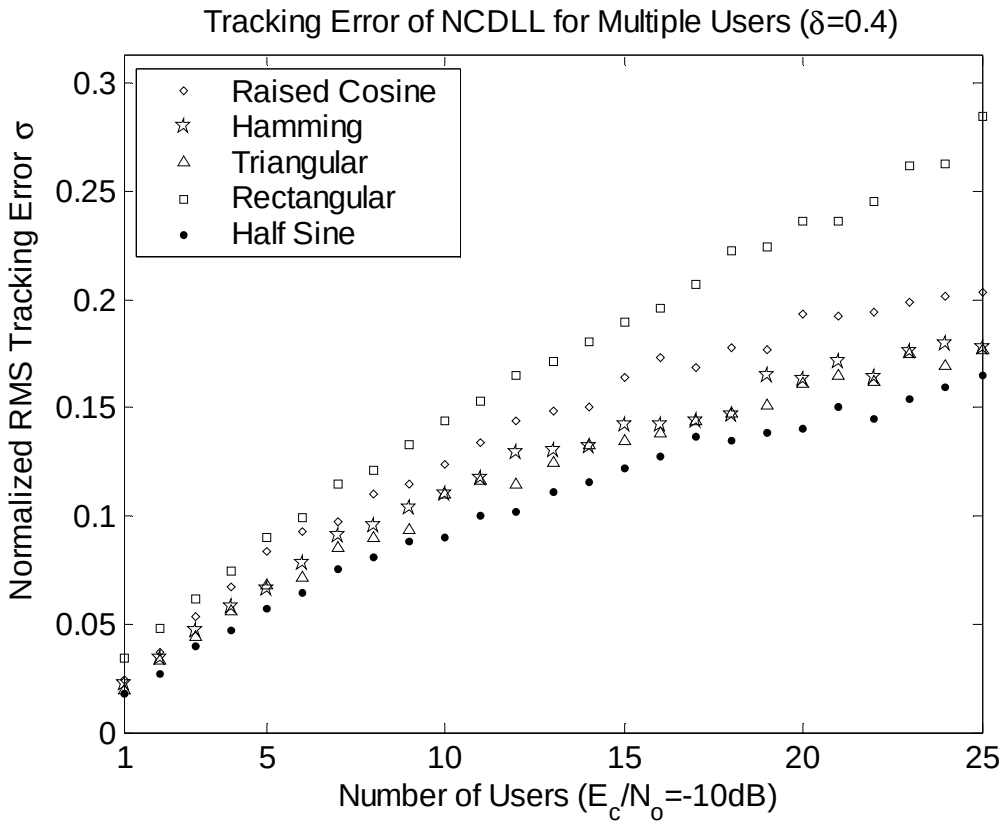

Figure 3-17 : Normalized RMS Tracking Error for Multiple Users at 0.4 Early-Late Discriminator Offset

TABLE 3-6 : NUMBER OF USERS MAINTAINED AT σ = 0.15 FOR δ = 0.4

PULSE SHAPE	NO OF USERS
Raised Cosine	14
Hamming	18
Triangular	19
Rectangular	11
Half-Sine	21

3.5 Tradeoff Mean-time-to-lose-lock and Tracking Jitter

From the previous discussion, it is observed that using an early late discriminator offset other than $\delta = 0.5$ can either increase or decrease the NCDLL slope thereby decreasing or increasing the RMS tracking error. All the nonrectangular pulse shapes have a maximum slope around $\delta = 0.2$. In order to use pulse shapes other than the ideal rectangular and guarantee a better performance compared to the rectangular, NCDLL discriminator offset must necessarily be less than 0.5. All the pulse shapes considered have a greater slope compared to the rectangular at offset less than 0.4 for example.

Using less offset however has its impact on the mean time to lose lock (MTTL). The MTTL essentially depends on the area under the S-curve $U(\varepsilon)$. From Figure (3-12) the area under the S-curve reduces considerably with an offset less than 0.5. The normalized MTTL ($B_L T$) against DLL spacing (δ) is shown for the noncoherent DLL is Figure (3-16). It is observed that for less discriminator offset, the MTTL decreases. The rectangular pulse shape has the most MTTL for all the pulse shapes at spacing above 0.5. For the Half-sine pulse in particular, using a spacing of 0.4 not only guarantees a greater S-curve slope and less RMS tracking error, but also guarantees greater MTTL compared to Rectangular at that particular spacing with an overall reduction in MTTL of 11%. Other pulse shapes have better MTTL comparable to the Rectangular pulse shape at δ = 0.35 for Triangular, 0.32 for Hamming and 0.22 for the Raised Cosine.

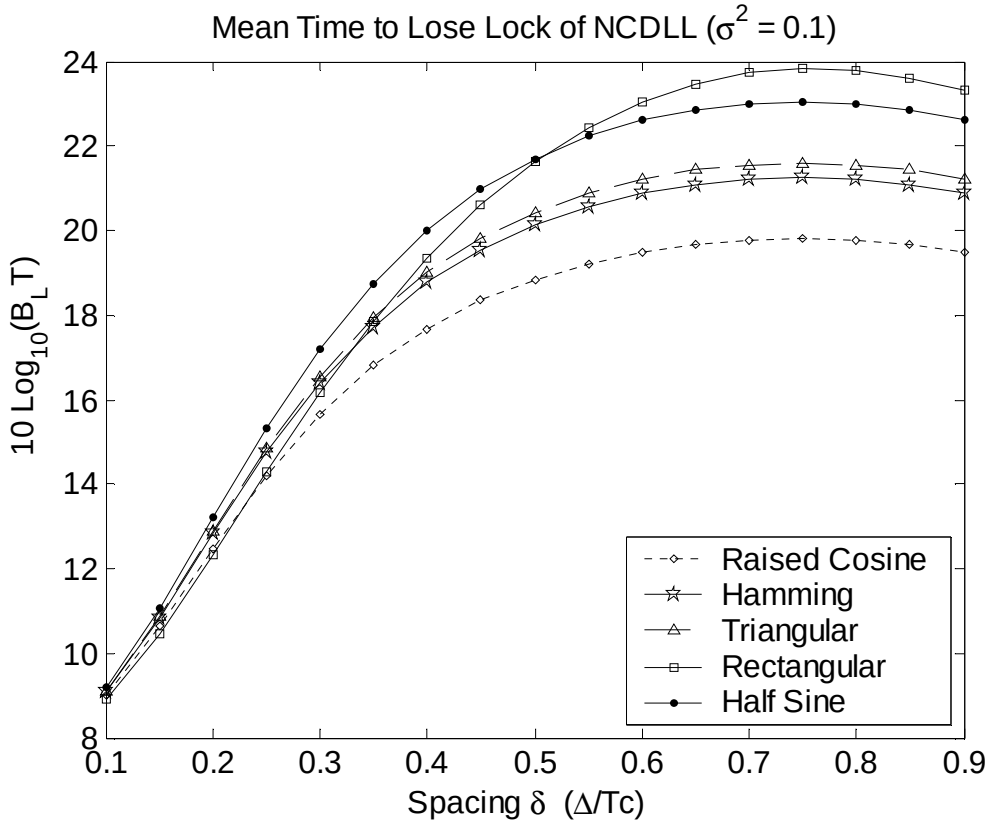

Figure 3-18 : Mean-Time-to-Lose-Lock for NCDLL versus Early-Late Discriminator Offset

3.6 Summary and Conclusion

Tracking jitter as a measure of the performance of the NCDLL has been shown to depend directly on the variance of the multiple access interference and inversely on the slope of the loop error characteristic (S-curve) at the origin. Five pulse shapes were considered. Both the variance of the multiple access interference and the slope of the S-curve at the origin were quantified for all five pulse shapes. Simulation in an AWGN channel has been used to show the different performance of the different pulse shapes. For the popular choice of early-late discriminator offset of 0.5, the Half-Sine pulse shape is seen to exhibit the best performance while the Raised-Cosine is observed to have the worse performance. Performance degradation in fading environment is noticed though the relative performance of the pulse shapes remains unchanged. Their performance in the presence of multiple users is also shown. At a fixed RMS tracking error of 0.15, a gain of up to 10 extra users is observed from the Half-Sine pulse shape compared to the Raised-Cosine pulse shape with a gain of 3 users over the Rectangular pulse shape. The effect of varying the early-late discriminator offset is shown to change the performance of the pulse shape by changing their respective slopes at the origin of the S-curve. Slightly reducing the offset to 0.4 makes all the nonrectangular pulse shapes outperform the rectangular pulse shape with an increase of up to 10 extra users from the Half-Sine compared to the Rectangular pulse shape. The tradeoff incurred from reducing the offset on the mean-time-to lose lock has also been presented with the observation that there is need for a balance in the benefits on performance one hand from reducing the early-late discriminator offset and the costs on the other hand for the mean-time-to lose lock.

Chapter 4

DLL Optimization

This chapter presents the approach of finding the optimal pulse shape for the noncoherent delay lock loop. The optimization problem is formulated. The approach to solving it pursued using special functions called Prolate Spheroidal Wave Functions. The optimization problem reduced to discrete form and solved using standard numerical packages. Results are shown for pulse shapes based on different bandwidth confinement. The proximity of classical pulse shapes to the optimum is also presented.

4.1 Problem Formulation

We seek to find the chip waveform with optimum tracking capabilities in terms of minimum RMS tracking error for the noncoherent DLL discussed in the previous chapter. The RMS tracking error σ from Equation (3-21) is $\sigma = \frac{\sqrt{2} I_o}{N E_c \kappa}$. Using the choice for the time difference between the early and the late discriminator channels $\delta = \frac{\Delta}{T_c} = \frac{1}{2}$, κ from Equation (3-36) is:

$$\kappa = 16\left[\int_{-\infty}^{+\infty} |H(f)|^2 \cos(\pi f) df\right]\left[\int_{-\infty}^{+\infty} 2\pi f |H(f)|^2 \sin(\pi f) df\right] \qquad (4\text{-}1)$$

Combining Equation (4-1) with the multiple-access interference variance from Equation (3-28), the RMS tracking error is:

$$\sigma = \frac{\sqrt{2}\int_{-\infty}^{+\infty} |H(f)|^4 df}{N E_c \, 16\left[\int_{-\infty}^{+\infty} |H(f)|^2 \cos(\pi f) df\right]\left[\int_{-\infty}^{+\infty} 2\pi f |H(f)|^2 \sin(\pi f) df\right]} \qquad (4\text{-}2)$$

The wave-dependent term in the RMS tracking error therefore is a function of $\frac{I_o}{\kappa}$. The objective is to minimize this function over functions $H(f)$. In designing chip waveforms with optimum tracking capabilities for the noncoherent DLL, additional signal constraints including fixed signal energy and limited bandwidth occupancy will be considered. Earlier work on the minimization of timing jitter in the coherent delay lock loop was done in [32]. The method developed in [32] is closely followed and applied to the

noncoherent delay lock loop considered in this work. Neglecting all constant terms from the RMS tracking error, we get a cost function F as:

$$F = \frac{\int_{-\infty}^{+\infty} |H(f)|^4 df}{\left[\int_{-\infty}^{+\infty} |H(f)|^2 \cos(\pi f) df\right]\left[\int_{-\infty}^{+\infty} 2\pi f |H(f)|^2 \sin(\pi f) df\right]} \quad (4\text{-}3)$$

The objective is to minimize this function subject to additional constraint of normalized chip energy requirement specified by:

$$\int_{-\infty}^{\infty} |H(f)|^2 df = 1 \quad (4\text{-}4)$$

In addition, the bandwidth occupancy of the chip waveform is confined so that only a small fraction η of its energy spills over a given range $[-B, B]$. This is always advantageous in any communication system from the point of view of error performance as the error performance depends on the amount of energy in the chip waveform. In direct-sequence spread spectrum systems, a bandwidth efficient chip waveform will allow for the use of a higher spreading factor N for a given allocated spectrum, thereby improving the overall system performance. The constraint for bandwidth confinement is:

$$\int_{-B}^{B} |H(f)|^2 df = 1 - \eta \quad (4\text{-}5)$$

Taking the two constraints above into consideration, the optimization problem is formulated as follows:

$$\textit{Minimize} \quad F = \frac{\int_{-\infty}^{+\infty} |H(f)|^4 \, df}{\left[\int_{-\infty}^{+\infty} |H(f)|^2 \cos(\pi f) df\right]\left[\int_{-\infty}^{+\infty} 2\pi f |H(f)|^2 \sin(\pi f) df\right]} \qquad (4\text{-}6)$$

$$\textit{Subject to} \quad \begin{cases} \int_{-\infty}^{\infty} |H(f)|^2 \, df = 1 \\ \int_{-B}^{B} |H(f)|^2 \, df = 1 - \eta \end{cases}$$

4.2 Approach to Solution

A direct, closed-form solution to this constrained optimization problem is not tractable. Instead the problem is converted to an equivalent discrete formulation with reduced dimensionality. This will be achieved by expanding the chip pulse Fourier transform $H(f)$ using an adequate set of basis functions, and then solving for the expansion coefficients that minimize the objective function F, subject to the constraints. Special functions known as Prolate Spheroidal Wave Functions [38] are particularly well suited for this and have been successfully used in [30, 31] for similar optimization problems.

4.2.1 Prolate Spheroidal Wave Functions

Prolate Spheroidal Wave functions (PSWF), denoted by $\{\Phi_n(f)\}$, have associated positive eigenvalues $\{\lambda_n\}$, and are constructed with finite time support T_c limited for symmetry to $[-T_c/2, T_c/2]$. They satisfy the kernel equation [38]:

$$\frac{1}{T_c}\int_{-B}^{B}\frac{\sin(f-u)}{f-u}\Phi_n(u)du = \lambda_n\Phi_n(f) \qquad (4\text{-}7)$$

and have the following two properties [38]:

$$\int_{-\infty}^{\infty}\Phi_m(f)\Phi_n(f)df = \delta_{mn} \qquad (4\text{-}8)$$

and

$$\int_{-B}^{B}\Phi_m(f)\Phi_n(f)df = \lambda_n\delta_{mn} \qquad (4\text{-}9)$$

where $\Phi_n(f)$ is a Prolate Spheroidal Wave Function of order n, δ_{mn} is the Kronecker delta symbol equal to 1 for $m=n$ and 0 otherwise and λ_n is the positive eigenvalue corresponding to the PSWF $\Phi_n(f)$. From Equation (4-8), the PSWF form a complete, orthonormal set over the space of finite-energy functions and from Equation (4-9) they form a complete, orthogonal set over the space of finite-energy functions in the interval $[-B, B]$.

It can further be concluded based on Equation (4-8) and (4-9) that pulse waveform designs based on PSWF possess a number of characteristics namely:

1. The pulse waveforms are doubly orthogonal to each other.
2. Pulse-width and bandwidth can be simultaneously controlled to match with arbitrary spectral mask.
3. Pulse-width can be kept constant regardless of the pulse order n.

In addition, it is found that the functions $\{\Phi_n(f)\}$ are even for n even and odd for n odd. Another important feature of the wave functions $\{\Phi_n(f)\}$ is that, among all time-limited functions with support T_c, they achieve the highest energy concentration in the band $[-B, B]$. This energy confinement is represented by the eigenvalues $\{\lambda_n\}$ (all smaller than 1) which are monotonically decreasing, and becoming negligible when the function's order n exceeds the time-bandwidth product $2BT_c$, as shown in [38]. These special features are the basis for using PSWF-based pulse waveform design for the optimized pulse shapes. They are very suitable for PN sequences used in a multiple access environment.

4.2.2 Problem Reduction

The above properties of PSWF work well in our case to reduce the complexity of the optimization problem. Since $\{\Phi_n(f)\}$ forms a complete set for the space of functions $H(f)$ of interest, the following expansion is obtained:

$$H(f) = \sum_{n=0}^{\infty} x_n \Phi_n(f) \qquad (4\text{-}10)$$

where x_n is given by the inner product $< H, \Phi_n >= \int_{-\infty}^{\infty} H(f)\Phi_n(f)df$. Since the eigenvalues $\{\lambda_n\}$ are rapidly decaying to zero, a truncated series expansion of the chip waveform function $H(f)$ involving only a limited number N of the orthonormal functions $\{\Phi_n(f)\}$ is used. In addition the functions $\Phi_n(f)$ have even symmetry and

therefore will have only even-indexed PSWF in its expansion. The truncated series becomes:

$$H(f) \cong \sum_{n=0}^{N} x_{2n} \Phi_{2n}(f) \tag{4-11}$$

Thus, with negligible impact on accuracy [32], this approach results in a discrete, finite-dimensional nonlinear optimization problem in terms of the expansion coefficients $\{x_{2n}\}$. The new form for the optimization problem becomes:

$$\textit{Minimize} \quad F = \frac{\sum_{n}^{N} \cdots \sum_{m}^{N} \gamma_1(n,\ldots,m) \prod_{n=0}^{N} x_{2n}}{\left[\sum_{n}^{N}\sum_{m=0}^{N} \gamma_2(n,m)\, x_{2n}\, x_{2m}\right]\left[\sum_{n}^{N}\sum_{m=0}^{N} \gamma_3(n,m)\, x_{2n}\, x_{2m}\right]}$$

$$\textit{Subject to} \quad \begin{cases} \sum_{n=0}^{N} x_{2n}^2 = 1 \\ \sum_{n=0}^{N} \lambda_{2n} x_{2n}^2 = 1-\eta \end{cases} \tag{4-12}$$

where the coefficients of the cost function to be minimized are given by:

$$\begin{aligned} \gamma_1(n,\ldots,m) &= (4;0,1,\ldots N) \int_{-\infty}^{\infty} \prod_{n=0}^{N} \Phi_{2n}(f)\, df \\ \gamma_2(n,m) &= \int_{-\infty}^{\infty} \Phi_{2n}(f)\, \Phi_{2m}(f) \cos(\pi f)\, df \\ \gamma_3(n,m) &= \int_{-\infty}^{\infty} 2\pi f\, \Phi_{2n}(f)\, \Phi_{2m}(f) \sin(\pi f)\, df \end{aligned} \tag{4-13}$$

with $(4;0,1,\ldots,N)$ denoting the multinomial coefficient equal to $4!/(0!1!\ldots N!)$.

This approach results in a discrete, finite-dimensional nonlinear optimization problem in terms of the expansion coefficients x_{2n} which is solved using standard numerical optimization methods. Numerical analysis packages are used to generate the Prolate Spheroidal Wave Functions.

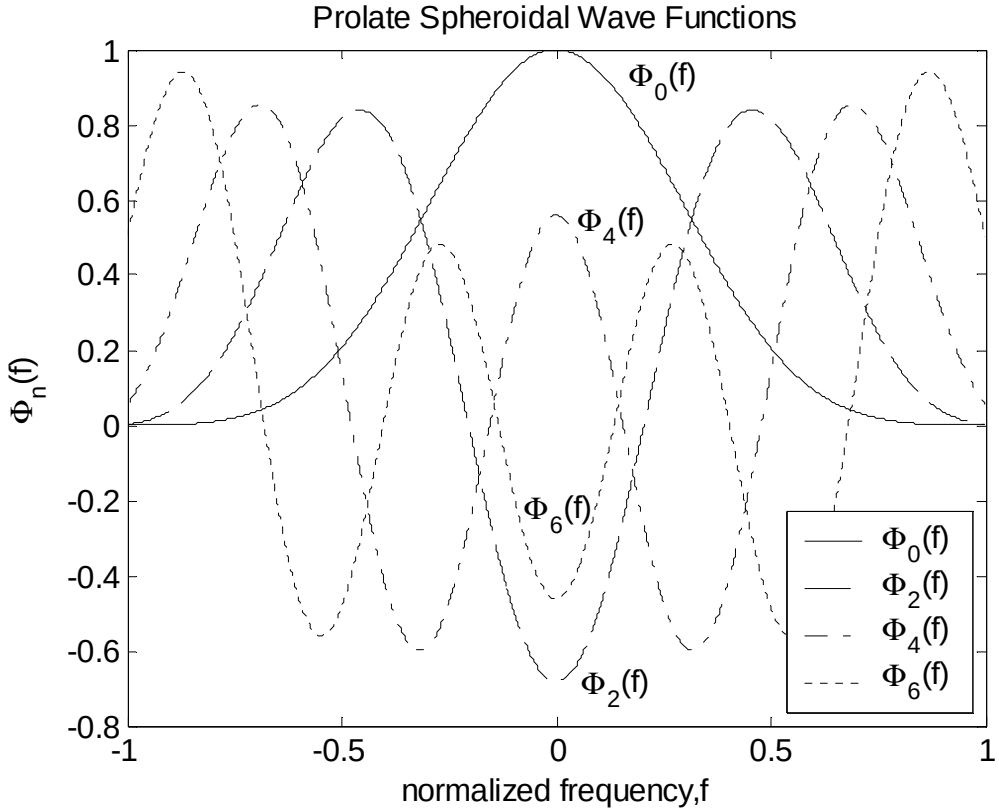

Figure 4-1 : Prolate Spheroidal Wave Functions

TABLE 4-1 : EIGENVALUES OF PROLATE SPHEROIDAL WAVE FUNCTIONS FOR VALUES OF BT_c

BT_c	Eigenvalues					
	λ_0	λ_2	λ_4	λ_6	λ_8	λ_{10}
1	9.8100E-01	2.4360E-01	1.0660E-03	4.8030E-07	5.9719E-11	2.8431E-15
2	9.9990E-01	9.6740E-01	2.7470E-01	3.4782E-03	7.4656E-06	5.8204E-09
3	9.9990E-01	9.9750E-01	9.1760E-01	3.3390E-01	5.9345E-03	2.6294E-05

4.3 Design Examples

The approach to obtaining these optimized pulses is based on maintaining a given bandwidth occupancy that is typically the same as that of the best performing conventional pulse and then attempting to solve the optimization problem until a feasible solution that minimizes the cost function F is found.

For the range of bandwidth of interest of $1BT_c$ to $2BT_c$, the eigenvalues λ_{2n} of the PSWF are strictly decreasing and fall rapidly towards zero with increasing n [30] shown in Table (4-1). We therefore truncate our series expansion to N=3 and use the first four even PSWF (n=0:3) shown in Figure (4-1) for our solution.

Numerical results for the solution of the optimization problem are given in Table (4-2). Comparison is made between the conventional pulse shapes and the optimized pulse shapes. In-band power bandwidth measures of 99% and 99.9% are used which corresponds to η equal to 1% and 0.1% in Equation (4-5). Two samples of optimized pulse shapes are given in Table (4-2) referred to as OPT1 and OPT2, respectively. Their expansion coefficients x_{2n} are given in Table (4-3).

With regard to the 99% bandwidth, the Half-Sine pulse has the lowest bandwidth of $1.18/T_c$ and is used to design OPT1 shown in Figure (4-2). Similarly, when considering the 99.9% bandwidth, the Hamming pulse has the lowest bandwidth of $1.6/T_c$ and is used to design OPT2 shown in Figure (4-3)

TABLE 4-2 : PERFORMANCE COMPARISONS FOR DIFFERENT PULSE SHAPES

PULSE SHAPE	99% BW BT_c	99.9% BW BT_c	I_o	κ	COST FUNCTION $F = I_o / \kappa$
Raised Cosine	1.4098	1.7300	0.24055	0.8889	0.27062
Hamming	1.3044	1.6051	0.26368	1.3570	0.19431
Triangular	1.3005	3.1125	0.26964	1.5000	0.17976
Rectangular	6.3539	13.6842	0.33333	2.0000	0.16667
Half Sine	1.1833	2.7337	0.29332	2.0000	0.14666
OPT1	1.2000	4.6942	0.3157	2.4200	0.13045
OPT2	1.1950	1.6000	0.2838	1.7735	0.16002

In Figure (4-4) the cost function F is plotted against the normalized bandwidth BT_c for various conventional and the optimized pulse shapes. The figure shows the proximity of the Half-Sine to the optimal curve. OPT1 has a slight RMS tracking improvement over the Half-Sine pulse shape showing that the Half-Sine is quasi optimum. Figure (4-5) shows the plot of the cost function F against the normalized bandwidth BT_c for 99.9% bandwidth. The proximity of the Hamming pulse shape to the optimal curve demonstrates that the Hamming pulse shape is closest to optimal when considering 99.9% bandwidth occupancy.

TABLE 4-3 : EXPANSION COEFFICIENTS OF OPTIMIZED PULSE SHAPES

OPTIMIZED PULSE SHAPE	x_0	x_2	x_4	x_6
OPT1	0.9971530493	-0.0653625421	0.0191688443	0.0323433081
OPT2	0.9990092246	-0.0444985504	0.0006632119	0.0000873278

$$H_{OPT}(f) \cong x_0\Phi_0(f) + x_2\Phi_2(f) + x_4\Phi_4(f) + x_6\Phi_6(f)$$

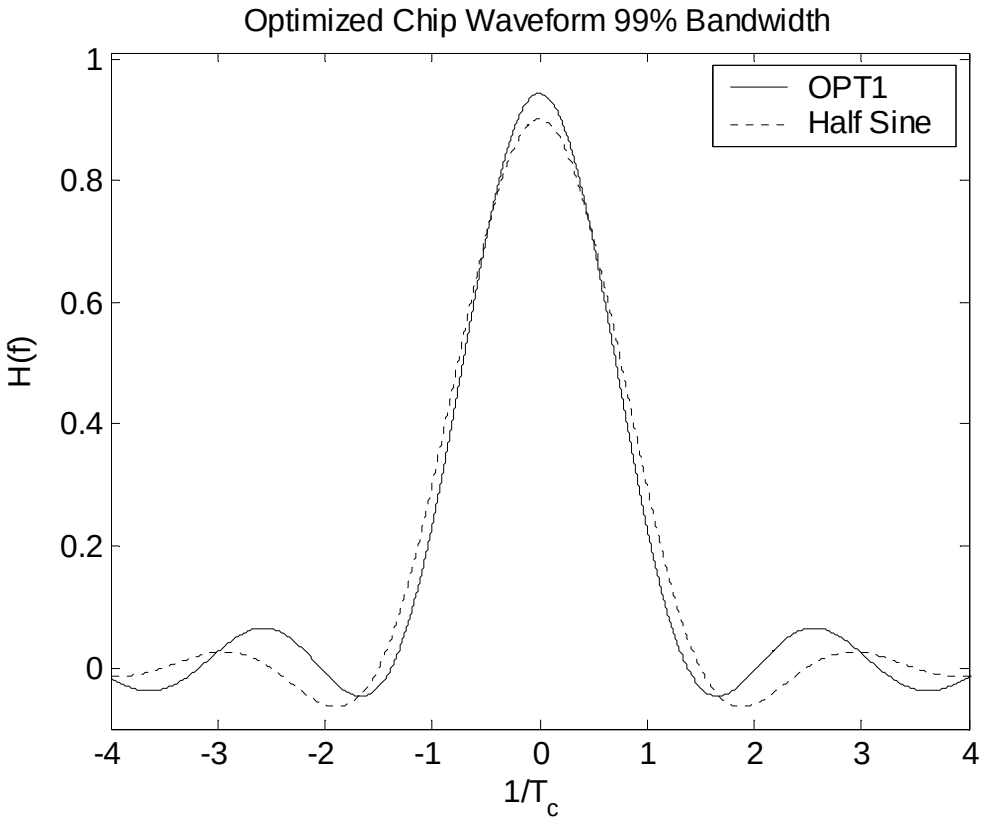

Figure 4-2 : Frequency Domain Representation of Optimized Pulse Shape OPT1 compare to the Half Sine Pulse Shape.

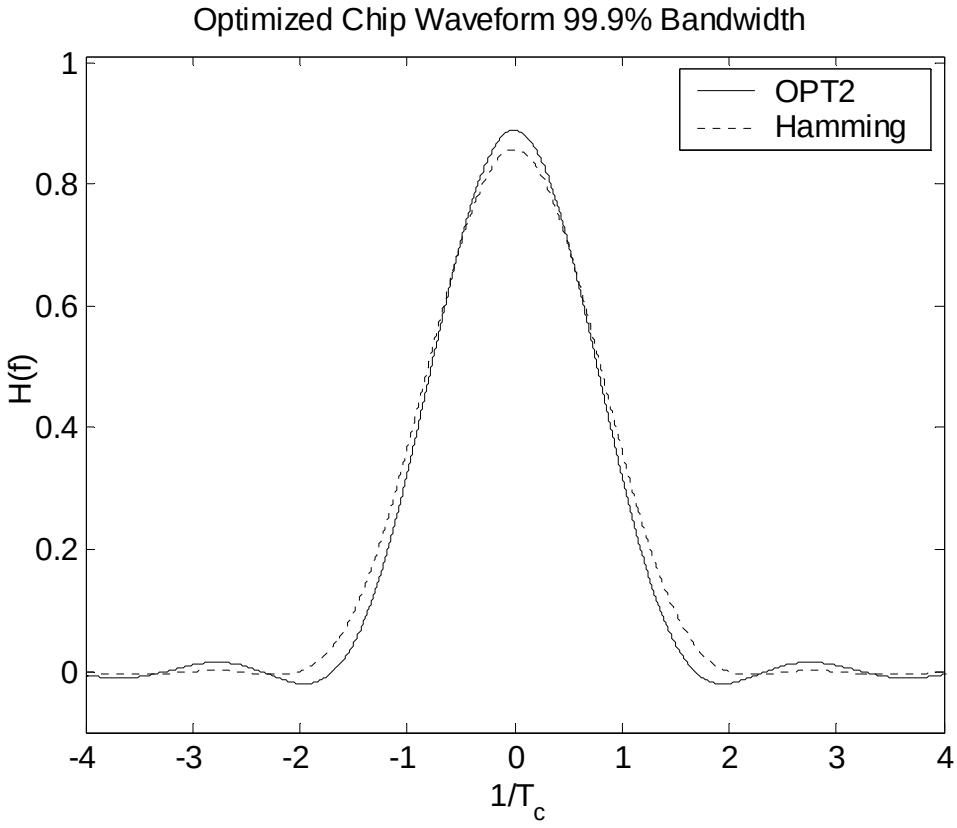

Figure 4-3 : Frequency Domain Representation of Optimized Pulse Shape OPT2 compared to the Hamming Pulse Shape

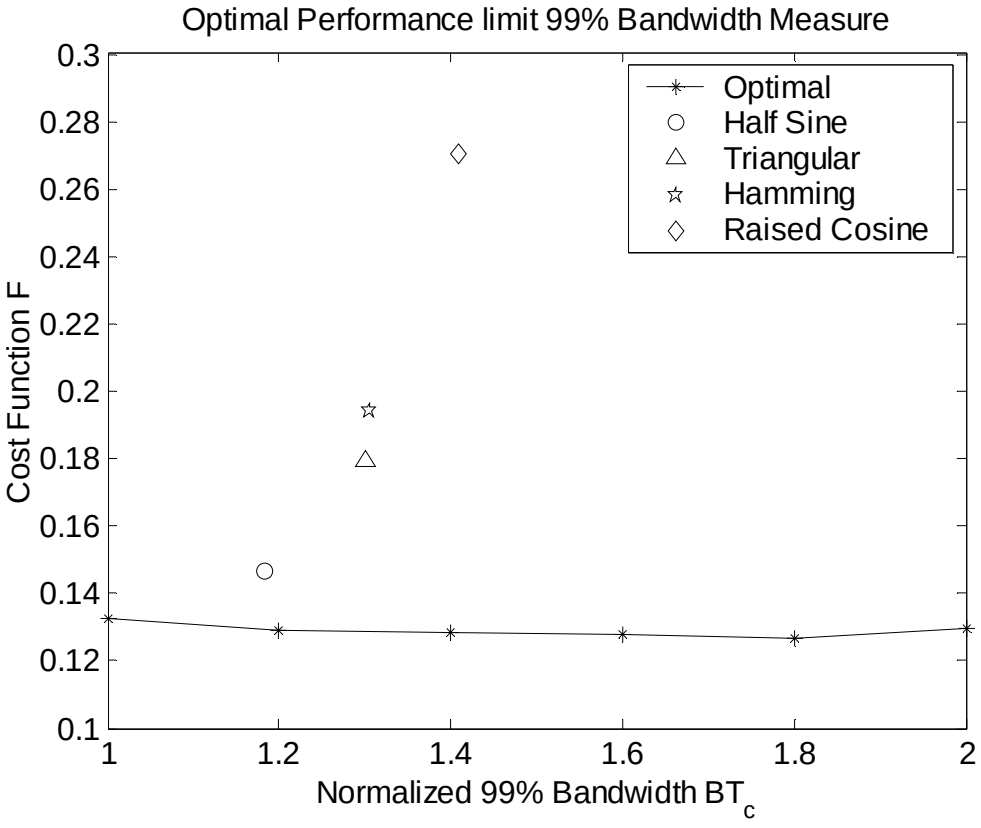

Figure 4-4 : Optimal Performance Limit 99% Bandwidth Measure

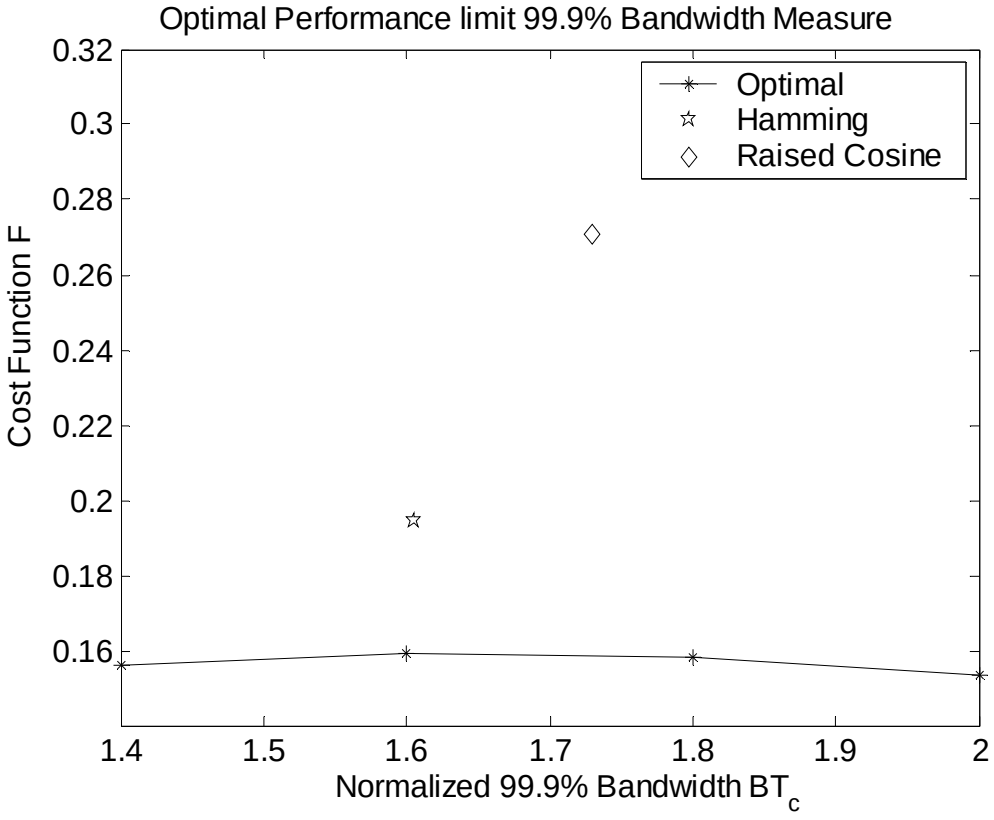

Figure 4-5 : Optimal Performance Limit 99.9% Bandwidth Measure

4.4 Summary and Conclusion

The problem of finding the pulse shape with optimum tracking capabilities in terms of minimum tracking jitter is carried out in this work. The problem was reduced to discrete form using Prolate Spheroidal Wave Functions as a basis because of their special properties the most important of which is that they achieve the highest energy concentration within any band limit. Optimum pulse shapes were designed using the bandwidth confinement of classical pulse shapes as benchmarks. The results indicate that the Half-Sine pulse shape is quasi-optimum when considering 99% bandwidth confinements while the Hamming pulse shape is closest to the optimum when considering 99.9% bandwidth confinement. The Hamming pulse shape is however not as close to the Half-Sine considering their respective bandwidth confinements.

Chapter 5

DSP Implementation

The proposed scheme is implemented using a digital signal processor (DSP). The implementation is to show the practicability of such a scheme and how it can be implemented in hardware. This chapter discusses this approach with some results on the tradeoff between accuracy in performance and DSP resource.

5.1 Introduction to DSP

A DSP is basically a processor whose hardware, software, and instruction sets are optimized for high-speed numeric processing applications, essential for processing digital data representing analog signals [39]. What a DSP does is to receive digital values based

on samples of a signal, calculates the results and provides digital values that represent the output. The DSP high-speed arithmetic and logical hardware is programmed to rapidly execute algorithms modeling analog functions.

Real world signals are analog. DSPs are additional tools for handling analog signals. Figure (5-1) shows a typical Analog/DSP system. To make use of the DSP, the analog input signal is converted to digital through an analog to digital converter (ADC). Before this, the signal is filtered through a low pass filter to cut off frequencies higher than about half the maximum frequency of interest (Nyquist frequency). The low pass filter used is named an anti-aliasing filter because it prevents aliasing (components appearing to have a frequency lower than their true value) of high frequency components. When the signal processing is completed, the output is the converted back to an analog signal through a digital to analog converter (DAC). The output signal is made up of impulses which contain all frequencies. This output is also low pass filtered to remove components above the Nyquist frequency. The low pass filter used is named an anti-imaging filter. Both the anti-aliasing and anti-imaging filter have similar characteristics.

The main reason for the increased use of DSPs today is that it enhances existing products at low cost and opens doors to new products not possible before. DSP processors offer tremendous low-cost computing capability. With a DSP it is easy to change, manipulate, correct and update applications. DSPs are more tolerant to temperature, voltage changes and mechanical vibration. In addition DSP reduce noise susceptibility and in certain applications may reduce chip count and power consumption.

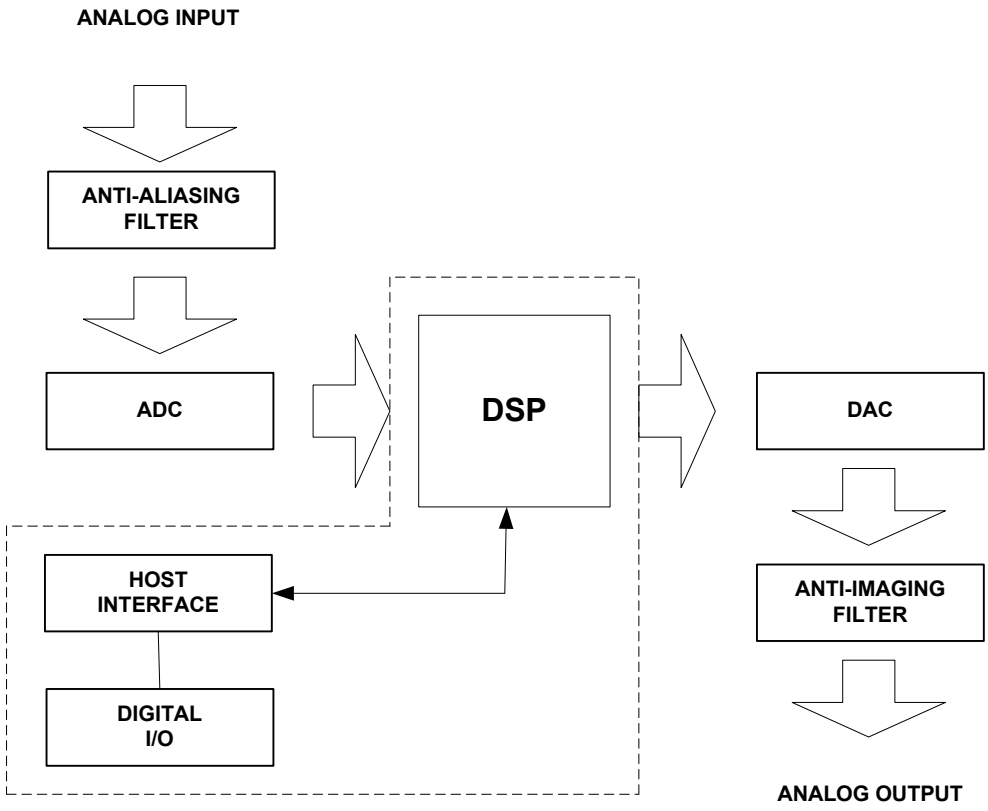

Figure 5-1 : Analog/DSP System

Some disadvantage however is that DSP designs can be expensive for high bandwidth signals where fast analogue/digital conversion is required. Design of DSP systems is also a time-consuming, highly complex and specialized activity.

In the area of wireless systems and networks, the use of DSP has made it possible to reduce base station size, reduce the number of components required to achieve functionality, make the station upgradeable in place by means of software and reduce station power consumption all at low cost. DSP have therefore become a standard for testing and implementing communication system algorithms.

5.2 System Description

A digital code tracking loop is implemented on the Texas instrument TMS3206713 (Appendix B). The block diagram of the system implemented is shown in Figure (5-2). The loop consists of input buffer, PN code generator, pulse shaper and early-late correlators. The tracking loop VCO is implemented using a numerically controlled oscillator. The scheme is implemented on the assumption that the received signal $r(n)$ is already sampled so the need for an ADC and a DAC are eliminated. The sampled received signal is passed straight into the DSP from the host PC through the input buffer and tracking is performed to obtain the tracking delay. A PN code generator is programmed to generate random signature sequences of $\{\pm 1\}$ for each user. The received signal is correlated with an early and late version of the generated PN code in accordance with code tracking loop model. The sum of product (SOP) is the key element in most

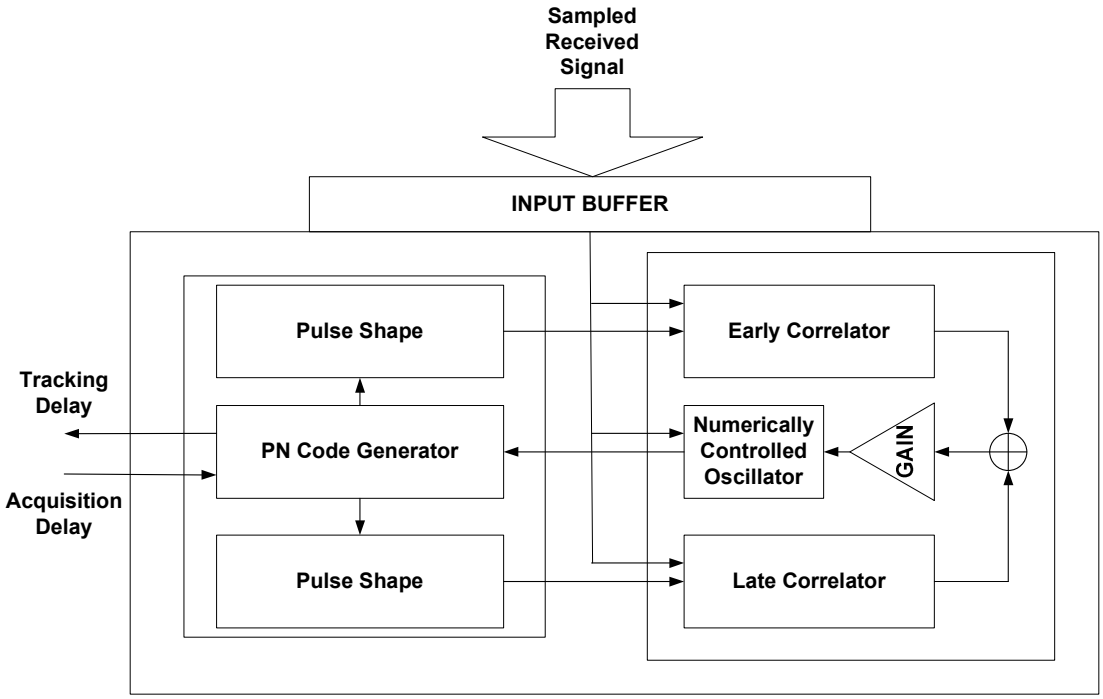

Figure 5-2 : Tracking Loop Implementation Block Diagram

DSP algorithms. DSP processors are optimized to perform multiplication and addition efficiently in one cycle. The correlator for the DSP is essentially a multiply and add circuit implementation (MAC). The difference of the correlated outputs is passed through a first order digital filter with a gain representing the voltage-to-frequency conversion. The output is used to drive the numerically controlled oscillator that acts to shift the PN sequence generator forward or backwards depending on the correction applied. The generated PN sequence is up sampled and pulse shaped using the appropriate pulse shape at the pulse shaper block. The numbers of samples are taken at 8, 16, 32, and 64 times. The output of the DSP is the delay estimate which is fed back into the host PC for comparison with the actual delay and calculation for the tracking jitter is done. This subsystem of the entire CDMA receiver assumes an initial input from an acquisition subsystem which feeds in the initial estimate of delay to within a chip period.

5.3 Test Results

A primary issue with digital implementation is the performance degradation that may arise from sampling and quantization. The tracking loops earlier discussed have used different pulse shapes. Each pulse shape has been sampled appropriately. It is however impossible to take samples at every point to completely characterize the pulse shape. We investigate the effect of this digital sampling on the performance of the tracking loop for different pulse shapes using the DSP implementation.

The number of samples taken was 8, 16, 32, and 64 for each pulse shape. Table (5-1) and Figure (5-3) show the normalized RMS tracking error σ for the various pulse shapes at a fixed noise level $E_c / N_o = -10\,dB$ for various numbers of samples per pulse. It is observed that taking more samples per pulse shape decreases the RMS tracking error thereby increasing the performance of the tracking loop. The misadjustment becomes less as more samples are taken because the estimate of the delay becomes slightly more accurate than with less number of samples. The rectangular pulse shape on the other hand does not benefit from taking more samples because its shape is flat.

Taking more number of samples has its toll on the amount of resources needed. Figure (5-4) shows the amount of time needed in milliseconds at a DSP clock rate of 225 MHz (Appendix B) obtained from the DSP CPU cycles. It is desirable to achieve lock in the minimum amount of time possible otherwise return the system to the acquisition stage. Depending on the requirements of the system as a whole, designers can chose the number of samples for the fastest amount of lock time with a compromise on tracking jitter accuracy. Figure (5-5) shows the memory requirements of the test system (Kb). DSP have very limited memory compared to general purpose processors therefore another compromise is necessary on the accuracy of the tracking jitter based on the memory available. Based on the results obtained sampling at 16 samples per pulse shape is a good enough compromise between tracking jitter accuracy and resource requirements for the optimized pulse shapes because taking samples greater than 16 samples per pulse has little effect on the tracking jitter compared to the additional requirements of memory and time to lock.

TABLE 5-1 : TRACKING JITTER FOR VARIOUS SAMPLES PER PULSE AT $E_c / N_o = -10\,dB$

PULSE SHAPE	8	16	32	64
Raised Cosine	0.14068	0.10157	0.05760	0.03766
Hamming	0.07919	0.04595	0.02875	0.02564
Triangular	0.06113	0.03609	0.02785	0.02181
Rectangular	0.04911	0.04916	0.05181	0.05666
Half Sine	0.03405	0.02294	0.01914	0.01721
OPT1	0.03269	0.02199	0.01869	0.01694
OPT2	0.03897	0.02640	0.02180	0.01966

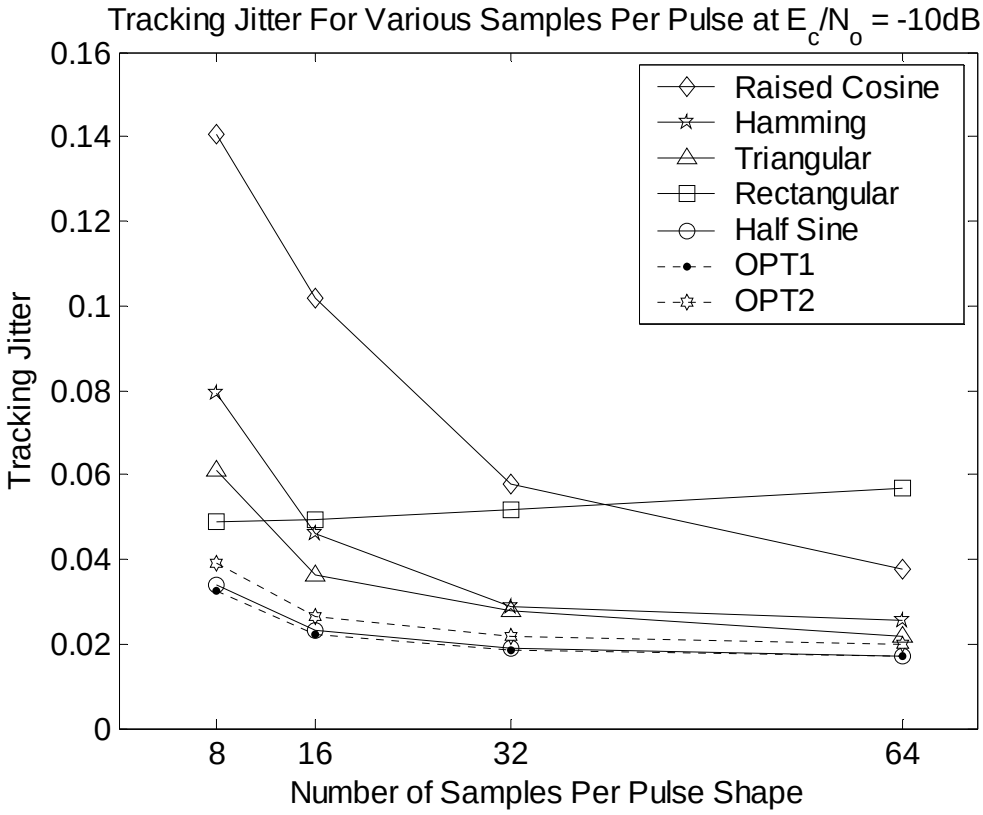

Figure 5-3 : Tracking Jitter for Various Samples Per Pulse at $E_c / N_o = -10dB$

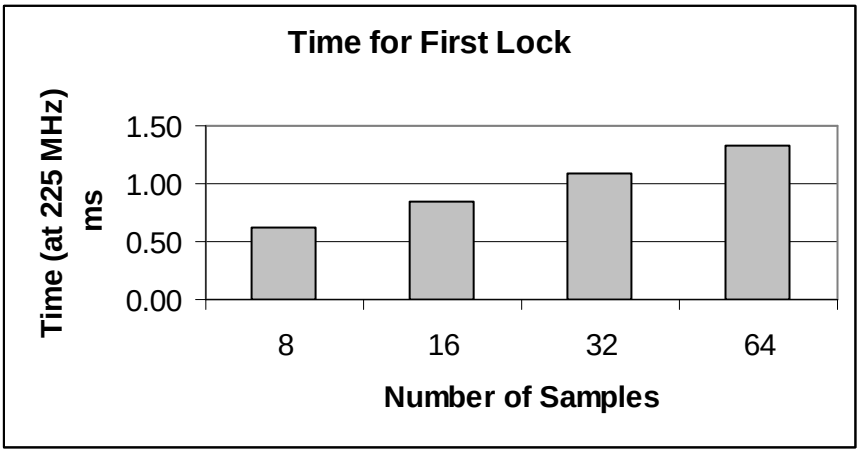

Figure 5-4 : Time in (ms) for first lock

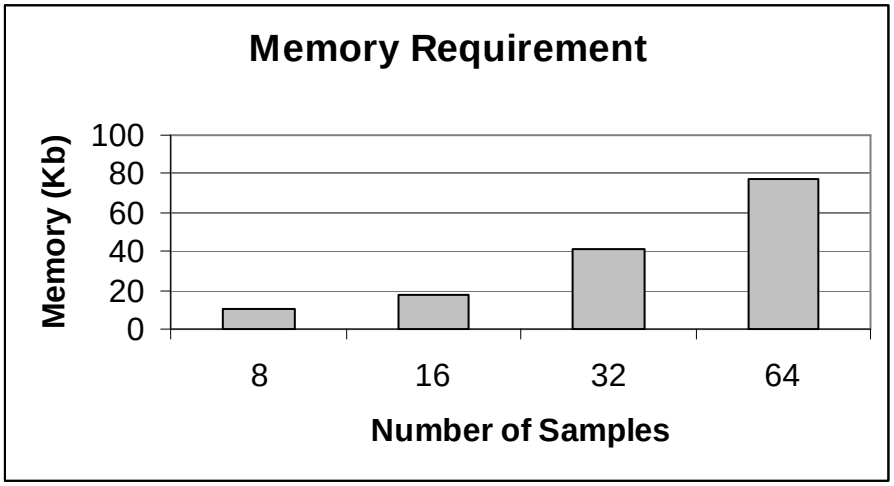

Figure 5-5 : Memory Requirement

5.4 Summary and Conclusion

A DSP system was implemented for the digital code tracking loop using Texas Instrument TMS3206713 DSK. Test results were obtained based on the number of samples taken per pulse. The performance of the pulse shapes remain unchanged though system designers have to make a compromise between the less tracking jitter and the amount of resources required in terms of the time to achieve the first lock and the memory available. For the best optimum pulse shape (OPT1), it is also observed that taking more samples makes its performance in hardware converge towards that of the Half-Sine illustrating the quasi optimality of the Half-Sine pulse shape. Based on the results obtained sampling at 16 samples per pulse shape is a good enough compromise between tracking jitter and resource requirements for the optimized pulse shapes. Taking samples greater than 16 samples per pulse has little effect on the tracking jitter compared to the additional requirements of memory and increase in time to lock.

Chapter 6

Conclusions and Recommendations for Future Work

6.1 Conclusions

The performance of the noncoherent delay lock depends directly as the variance of the multiple-access interference and inversely as the slope of the loop error characteristic s-curve at the origin. The performance of the loop is from here quantified for different pulse shapes. For the popular choice of early-late discriminator offset of 0.5, the Half-Sine pulse shape sports the best performance while the Raised-Cosine pulse shape exhibits the worse performance. The others are Rectangular, Triangular and Hamming pulse shapes in that order from best to worst. The coherent delay lock loop on the other

hand has the Rectangular as the worst performing pulse shape with early-late discriminator offset of 0.5.

The performance of the pulse shapes in the noncoherent delay lock loop does not remain constant with different early-late discriminator offset unlike the performance of the Rectangular pulse shape in the coherent delay lock loop. Changing the early-late discriminator offset has a significant impact on the performance of the pulse shapes; it may change the performance of each pulse shape relative to the other. All non rectangular pulse shape considered performs better than the Rectangular pulse shape at early-late discriminator offset of 0.4 and less.

The results of optimum pulse shapes designed in terms of minimum tracking jitter indicate that the Half-Sine pulse shape is quasi optimum with regard to 99% bandwidth confinement. In hardware implementation, taking more samples per chip tend to blur the performance difference between the Half-Sine and the best optimized pulse shape. The Half-Sine pulse shape can therefore be considered optimum for all practical purposes.

6.2 Recommendations for Future Work

This work has focused on the effect of full response pulses. A recommendation for future work will be to consider the effect of partial response pulses and study the additional effect of inter-symbol interference.

The loop filter considered in this work is assumed to be a first order loop filter. Some literatures have suggested that making this loop filter adaptive could increase the overall performance of the tracking loop. Work could be done to study the effect of various adaptive filter algorithms on the performance of the noncoherent delay lock loop.

Appendix

7.1 Appendix A: Derivation of Equation (3-1) and (3-17)

The analyses that follow use the noncoherent delay lock. To find the variance of the timing error τ we first proceed to find the variance of the discriminator output $z_{\Delta}(\tau)$. We consider first $z_1(\tau)$, with the statistics of $z_2(\tau)$ being similar. Assuming the total number of equal energy users k_u and the number of accumulated chips N are sufficiently large that we may take y_1^I and y_1^Q to be Gaussian random variables according to the central limit theorem approximation, following the analysis in [2], we may express them as:

$$\begin{aligned} y_1^I &= \sum_{n=1}^{N}\left[\sqrt{E_c}R_1\cos\phi + v_n^I\right] \\ y_1^Q &= \sum_{n=1}^{N}\left[\sqrt{E_c}R_1\sin\phi + v_n^Q\right] \end{aligned} \tag{7-1}$$

where:

$$R_1 = R(\tau+\Delta) \quad and \quad R_2 = R(\tau-\Delta)$$

v_n^I and v_n^Q are independent Gaussian random variables with zero mean and

$$\mathrm{var}\left[v_n^I\right] = \mathrm{var}\left[v_n^Q\right] = \frac{I_o}{2} \tag{7-2}$$

The mean and variance of $z_1(\tau)$ can then be obtained:

$$E(z_1) = E\left[(y_1^I)^2\right] + E\left[(y_1^Q)^2\right]$$

$$= N^2E_cR_1^2\cos^2\phi + E\left[\left(\sum_{n=1}^{N}v_n^I\right)^2\right] + N^2E_cR_1^2\sin^2\phi + E\left[\left(\sum_{n=1}^{N}v_n^Q\right)^2\right]$$

$$= N^2 E_c R_1^2 + 2N(I_o / 2)$$

$$E(z_1) = N\left(NE_c R_1^2 + I_o\right) \tag{7-3}$$

where $I_o = I/W$ is the noise density received by each user's demodulator with I the total interference power and W Hz is the entire spreading bandwidth. The variance:

$$E(z_1^2) = E\left[\{\ (y_1^I)^2 + (y_1^Q)^2\ \}^2\right] \tag{7-4}$$

$$E(z_1^2) = E[(y_1^I)^4] + 2E[(y_1^I)^2]E[(y_1^Q)^2] + E[(y_1^Q)^4] \tag{7-5}$$

as above where:

$$E[(y_1^I)^2] = N^2 E_c R_1^2 \cos^2\phi + NI_o / 2$$

$$E[(y_1^Q)^2] = N^2 E_c R_1^2 \sin^2\phi + NI_o / 2$$

For the fourth-power terms, since odd moments of v are zero,

$$E[(y_1^I)^4] = N^4 E_c R_1^4 \cos^4\phi + 6N^3(I_o/2)E_c R_1^2 \cos^2\phi + E\left[\left(\sum_{n=1}^{N} v_n^I\right)^4\right] \tag{7-6}$$

$$E[(y_1^Q)^4] = N^4 E_c R_1^4 \sin^4\phi + 6N^3(I_o/2)E_c R_1^2 \sin^2\phi + E\left[\left(\sum_{n=1}^{N} v_n^Q\right)^4\right] \tag{7-7}$$

The variable of v are independent and Gaussian with zero mean hence [2]:

$$E\left[\left(\sum_{n=1}^{N} v_n^I\right)^4\right] = 3\left[E\sum_{n=1}^{N}\left(v_n^I\right)^2\right]^2$$

$$E\left[\left(\sum_{n=1}^{N} v_n^I\right)^4\right] = 3(NI_o/2)^2 \tag{7-8}$$

Substituting:

$$E(z_1^2) = E[(y_1^I)^4] + 2E[(y_1^I)^2]E[(y_1^Q)^2] + E[(y_1^Q)^4]$$

$$E(z_1^2) = N^4 E_c^2 R_1^4(\cos^4\phi + \sin^4\phi) + 3N^3 I_o E_c R_1^2 + 3(NI_o)^2/2 + 2N^4 E_c^2 R_1^4 \cos^2\phi \sin^2\phi + (NI_o)^2/2 + N^3 I_o E_c R_1^2$$

$$E(z_1^2) = N^4 E_c^2 R_1^4 + 2[N^2 I_o^2 + 2N^3 I_o E_c R_1^2 \qquad (7\text{-}9)$$

From here we can find the variance of z_1:

$$Var(z_1) = E(z_1^2) - [E(z_1)]^2$$

$$Var(z_1) = N^4 E_c^2 R_1^4 + 2[N^2 I_0^2 + N^3 I_o E_c R_1^2] - [N^4 E_c^2 R_1^4 + N^2 I_o^2 + 2N^3 I_o E_c R_1^2]$$

$$Var(z_1) = (NI_o)^2 [1 + 2N(E_c / I_o) R_1^2] \qquad (7\text{-}10)$$

and

$$Var(z_2) = (NI_o)^2 [1 + 2N(E_c / I_o) R_2^2] \qquad (7\text{-}11)$$

And finally substituting we find the variance of $z_\Delta(\tau)$:

$$Var[z_\Delta(\tau)] = Var(z_1) + Var(z_2) = 2(NI_o)^2 \left[1 + N(E_c / I_o) R_1^2 + N(E_c / I_o) R_2^2\right]$$

$$Var[z_\Delta(\tau)] = Var(z_1) + Var(z_2) = 2(NI_o)^2 \left[1 + N(E_c / I_o)\left(R_1^2 + R_2^2 \right)\right]$$

The variance is therefore bounded by:

$$V_o = Var[z_\Delta(\tau)] \le 2(NI_o)^2 \left[1 + 2N(E_c / I_o)\right] \qquad (7\text{-}12)$$

and the expected value of $z_\Delta(\tau)$:

$$E[z_\Delta(\tau)] = E(z_1) - E(z_2) = N^2 E_c (R_1^2 - R_2^2) = N^2 E_c [R^2(\tau - \Delta) - R^2(\tau + \Delta)] \quad (7\text{-}13)$$

Equation (7-12) is used in Equation (3-17) and Equation (7-13) is used in Equation (3-1).

7.2 Appendix B: TMS320C6713 Digital Signal Processor

The TMS320C6713 (C6713) from Texas Instrument is a fast special-purpose microprocessor with a specialized type of architecture and an instruction set appropriate for signal processing. The C6713 is based on the very long instruction word (VLIW) architecture, which is very well suited for numerically intensive algorithms. The C6713 belongs to the family of C6x floating-point processors and is capable of both fixed and floating point processing.

7.2.1 Hardware and Software Requirements

The required hardware is a DSP starter kit (DSK) Figure (7-1). The DSK features the actual TMS320C6713 DSP at 225MHz. In addition, it features an Embedded USB JTAG controller with plug and play drivers, USB cable, TI TLV320AIC23 codec, 2M x 32 on board SDRAM, 512K bytes of on board Flash ROM, 3 Expansion connectors (Memory Interface, Peripheral Interface, and Host Port Interface), an onboard IEEE 1149.1 JTAG connection, 4 LEDs, 4 position dip switch and ± 5 Volt operation power supply.

A host PC is required. The recommended hardware configuration for the host PC is 128MB of RAM, SVGA (1024 x 768) color display and 500 MHz or faster Pentium or compatible. The DSK board connects to the USB port of the PC through the USB cable included.

To perform the simulation, familiarity with C programming language is required. The software tools needed to generate TMS320C6713 executable files is the Code Composer Studio (CCS). CCS incorporates the assembler, linker, compiler, simulator and debugger utilities. CCS is installed on the host PC and used to program the DSK.

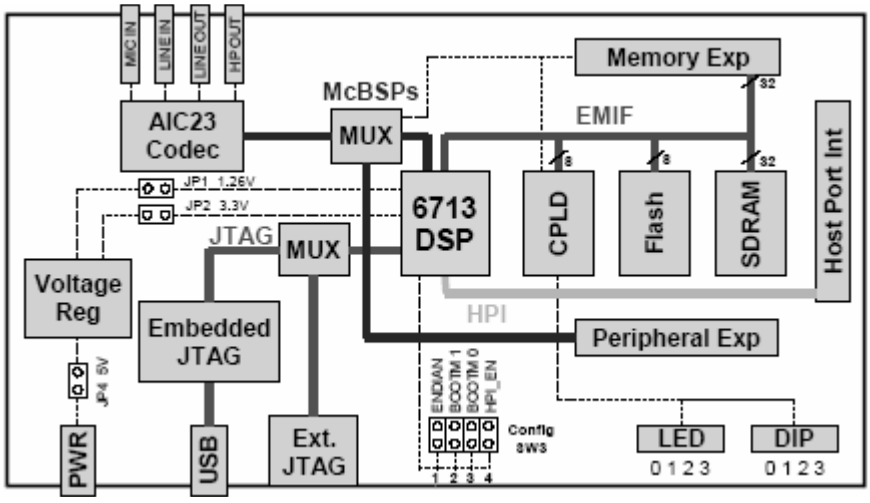

Figure 7-1 : TMS320C6713 Based DSK Block Diagram

Bibliography

[1] T. S. Rappaport, *Wireless Communications Principles and Practice*: Pearson Education Inc., 2002.

[2] A. J. Viterbi, *Principles of Spread Spectrum Communication*: Addison-Wesley, 1995.

[3] R. Prasad, *CDMA for Wireless Personal Communications*: Artech House Publishers, 1996.

[4] C. Huang, "An analysis of CDMA 3G wireless communications standards," presented at Vehicular Technology Conference, 1999 IEEE 49th, 1999.

[5] S. Glisic and B. Vucetic, *Spread Spectrum CDMA Systems for Wireless Communications*: Artech House Mobile Communications Series, 1997.

[6] J. G. Proakis, *Digital Communications*, 4 ed: McGraw-Hill Education, 2000.

[7] M. K. Simon, J. K. Omura, R. A. Scholtz, and B. K. Levitt, *Spread Spectrum Communications Handbook*: McGraw-Hill Inc, 1994.

[8] R. E. Ziemer, R. L. Peterson, and D. E. Borth, *Introduction to Spread Spectrum Communications*: Prentice Hall, 1995.

[9] J. J. Spilker and D. T. Magill, "The Delay-Lock Discriminator - An Optimum Tracking Device," *Proc. IRE*, vol. 49, pp. 1403-1416, 1961.

[10] J. J. Spilker, "Delay Lock Tracking of Binary Signals," *Space Electron Telem, IEEE Transactions on*, vol. SET-9, pp. 1-8, 1963.

[11] W. J. Gill, "A Comparison of Binary Delay-Lock Loop Implementation," *Aerosp Electron Syst, IEEE Transactions on*, vol. AES-2, pp. 415-424, 1966.

[12] M. Simon, "Noncoherent Pseudonoise Code Tracking Performance of Spread Spectrum Receivers," *Communications, IEEE Transactions on*, vol. 25, pp. 327-345, 1977.

[13] H. P. Hartmann, "Analysis of a Dithering Loop for PN Code Tracking," *Aerosp Electron Syst, IEEE Transaction on*, vol. AES-10, pp. 2-9, 1974.

[14] H. Meyr, "Nonlinear Analysis of Correlative Tracking Systems Using Renewal Process Theory," *Communications, IEEE Transactions on [legacy, pre - 1988]*, vol. 23, pp. 192-203, 1975.

[15] H. Meyr, "Delay-Lock Tracking of Stochastic Signals," *Communications, IEEE Transactions on [legacy, pre - 1988]*, vol. 24, pp. 331-339, 1976.

[16] W. Lindsey and H. Meyr, "Complete statistical description of the phase-error process generated by correlative tracking systems," *Information Theory, IEEE Transactions on*, vol. 23, pp. 194-202, 1977.

[17] A. Polydoros and C. Weber, "Analysis and Optimization of Correlative Code-Tracking Loops in Spread-Spectrum Systems," *Communications, IEEE Transactions on*, vol. 33, pp. 30-43, 1985.

[18] R. Yost and R. Boyd, "A Modified PN Code Tracking Loop: Its Performance Analysis and Comparative Evaluation," *Communications, IEEE Transactions on*, vol. 30, pp. 1027-1036, 1982.

[19] U. P. Bernhard, "Influence of data modulation and Doppler effects on the performance of a delay locked loop," presented at Spread Spectrum Techniques and Applications, 1994. IEEE ISSSTA '94., IEEE Third International Symposium on, 1994.

[20] A. Wilde, "Extended tracking range delay-locked loop," presented at Communications, 1995. ICC 95 Seattle, Gateway to Globalization, 1995 IEEE International Conference on, 1995.

[21] K. Jamaleddine, D. Vizireanu, F. Malassenet, and S. Halunga, "A new delay locked loop structure with enhanced tracking behavior," presented at Personal, Indoor and Mobile Radio Communications, 1996. PIMRC'96., Seventh IEEE International Symposium on, 1996.

[22] N.-Y. Yen, S.-L. Su, and S.-C. Hsieh, "Performance analysis of digital delay lock loops in the presence of Doppler shift," *Communications, IEEE Transactions on*, vol. 44, pp. 668-674, 1996.

[23] C.-Y. Lo, K.-C. Chen, and W.-H. Sheen, "Noncoherent DLL and TDL PN code tracking loops in Rayleigh fading channels," presented at Personal, Indoor and

Mobile Radio Communications, 1994. Wireless Networks - Catching the Mobile Future. 5th IEEE International Symposium on, 1994.

[24] W.-H. Sheen and G. L. Stuber, "Effects of multipath fading on delay-locked loops for spread spectrum systems," *Communications, IEEE Transactions on*, vol. 42, pp. 1947-1956, 1994.

[25] R. D. J. van Nee, "The Multipath Estimating Delay Lock Loop," presented at Spread Spectrum Techniques and Applications, 1992. ISSTA 92. IEEE Second International Symposium on, 1992.

[26] W.-H. Sheen and G. L. Stuber, "A new tracking loop for direct sequence spread spectrum systems on frequency-selective fading channels," *Communications, IEEE Transactions on*, vol. 43, pp. 3063-3072, 1995.

[27] A. Wilde, "Modified coherent PN-code tracking delay-locked loop," presented at Personal, Indoor and Mobile Radio Communications, 1994. Wireless Networks - Catching the Mobile Future. 5th IEEE International Symposium on, 1994.

[28] S. Thayaparan, T.-S. Ng, and J. Wang, "Half-sine and triangular despreading chip waveforms for coherent delay-locked tracking in DS/SS systems," *Communications, IEEE Transactions on*, vol. 48, pp. 1384-1391, 2000.

[29] X. Wu, C. Ling, and H. Xiang, "Despreading chip waveform design for coherent delay-locked tracking in DS/SS systems," presented at Communications, 2002. ICC 2002. IEEE International Conference on, 2002.

[30] M. A. Landolsi and W. E. Stark, "DS-CDMA chip waveform design for minimal interference under bandwidth, phase, and envelope constraints," *Communications, IEEE Transactions on*, vol. 47, pp. 1737-1746, 1999.

[31] T. Luo, S. Pasupathy, and E. S. Sousa, "Interference control and chip waveform design in multirate DS-CDMA communication systems," *Wireless Communications, IEEE Transactions on*, vol. 1, pp. 56-66, 2002.

[32] M. A. Landolsi, "Minimisation of timing jitter in CDMA code tracking," *Electronics Letters*, vol. 40, pp. 1352-1353, 2004.

[33] J. S. Lee and L. E. Miller, *CDMA Systems Engineering Handbook*: Artech House Publishers, 1998.

[34] K. S. Zigangirov, *Theory of Code Division Multiple Access Communication*: Wiley-IEEE Press, 2004.

[35] W. C. Lindsey, *Synchronization Systems in Communication and Control*: Prentice-Hall, 1972.

[36] J. Holmes and L. Biederman, "Delay-Lock-Loop Mean Time to Lose Lock," *Communications, IEEE Transactions on*, vol. 26, pp. 1549-1557, 1978.

[37] A. Wilde, "Mean time to lose lock for a coherent extended tracking range delay-locked loop," presented at Radio Receivers and Associated Systems, 1995., Sixth International Conference on, 1995.

[38] D. Slepian and H. O. Pollak, "Prolate Spheroidal Wave Functions, Fourier Analysis and Uncertainty," *Bell Sys. Tech.*, vol. 40, pp. 43-64, 1961.

[39] R. Chassaing, *Digital Signal Processing and Applications with the C6713 and C6416 DSK*: Wiley-Interscience, 2004.

VITA

Name: Ganiyu Babatunde HUSSAIN

Date of Birth: May 1976

Education: Bachelor Degree in Electrical and Electronic Engineering
University of Ibadan, Ibadan, Nigeria.
May 2000

Master Degree in Telecommunication Engineering
King Fahd University of Petroleum & Minerals
Dhahran, Saudi Arabia.
May 2005